DOI: 10.1002/chem.200701611

Application of MCD Spectroscopy and TD-DFT to Nonplanar Core-Modified Tetrabenzoporphyrins: Effect of Reduced Symmetry on Nonplanar Porphyrinoids**

John Mack,[a, b] Masaru Bunya,[a] Yusuke Shimizu,[c] Hiroki Uoyama,[d] Naoki Komobuchi,[c] Tetsuo Okujima,[c] Hidemitsu Uno,*[d] Satoshi Ito,[e] Martin J. Stillman,*[b] Noboru Ono,*[c] and Nagao Kobayashi*[a]

Abstract: The optical spectra of a series of core-modified tetrabenzoporphyrins were analyzed to determine the effects of core modification, ligand folding, and partial benzo substitution at the ligand periphery on the electronic structure by using magnetic circular dichroism (MCD) and NMR spectroscopy, X-ray crystallography, cyclic and differential pulse voltammetry, and TD-DFT calculations. Planar 21-carba-, 21-thia-, 21,23-dithia-, and 21-oxa-23-thiatetrabenzo[*b*,*g*,*l*,*q*]porphyrins reported previously were studied together with the previously unreported 21-oxa- and 21-carba-23-thiatetrabenzo-[*b*,*g*,*l*,*q*]porphyrins. The optical properties of these compounds are compared to those of tetrabenzo[*b*,*g*,*l*,*q*]-, 5,10,15,20-tetraphenyl-, 5,10,15,20-tetraphenyltetrabenzo[*b*,*g*,*l*,*q*]-21-thia-, 5,10,15,20-tetraphenyltetrabenzodithia-, 5,10,15,20-tetraphenyldibenzo[*g*,*q*]-21,23-dithia-, 5,10,15,20-tetraphenyldibenzo[*b*,*l*]-21,23-dithia-, 5,10,15,20-tetraphenyltribenzo[*g*,*q*,*l*]-21-thia-, and 5,10,15,20-tetraphenylbenzo[*b*]-21-thiaporphyrins. Michl's perimeter model and Gouterman's four-orbital model are used to conceptualize the results and to account for red shifts commonly observed in the spectral bands of nonplanar porphyrinoids.

Keywords: circular dichroism · density functional calculations · electronic structure · perimeter model · porphyrinoids

[a] Dr. J. Mack, M. Bunya, Prof. N. Kobayashi
Department of Chemistry
Graduate School of Science
Tohoku University
Sendai 980-8578 (Japan)
Fax: (+81) 22-795-7719
E-mail: nagaok@mail.tains.tohoku.ac.jp

[b] Dr. J. Mack, Prof. M. J. Stillman
Department of Chemistry
The University of Western Ontario
London, N6A 5B7 Ontario (Canada)
Fax: (+1) 519-661-3022
E-mail: martin.stillman@uwo.ca

[c] Y. Shimizu, N. Komobuchi, Dr. T. Okujima, Prof. N. Ono
Graduate School of Science and Engineering
Ehime University, Matsuyama 790-8577 (Japan)
Fax: (+81) 89-927-9615
E-mail: ononbr@dpc.ehime-u.ac.jp

[d] H. Uoyama, Prof. H. Uno
Integrated Center for Sciences (INCS)
Ehime University Matsuyama 790-8577
CREST, Japan Science and Technology Agency (Japan)
Fax: (+81) 89-927-9670
E-mail: uno@dpc.ehime-u.ac.jp

[e] Prof. S. Ito
Department of Applied Chemistry, Faculty of Engineering
Utsunomiya University, Utsunomiya 321-8585 (Japan)

[**] MCD = magnetic circular dichroism; TD-DFT = time-dependent density functional theory.

Supporting information for this article is available on the WWW under http://www.chemeurj.org/ or from the author.

Introduction

While the current focus in theoretical calculations on porphyrinoids is to interpret and understand the spectroscopic and electrochemical properties, a much greater challenge is to predict these properties given a specific structure. The electronic structure of porphyrinoids can be finely tuned to provide a set of properties suitable for use in specific practical applications by means of the wide range of possible structural modifications to the parent porphyrin ligand. The ability to predict the structure needed to achieve specific electronic properties is particularly important. For example, porphyrinoids designed for use in photodynamic therapy (PDT) of tumors[1] should have strong absorption bands in the red region (>650 nm) for light transparency in living cells. The electronic structure can be tuned by introducing electron-withdrawing and electron-donating groups[2] or sterically hindered bulky substituents,[3] by lowering the molecular symmetry by partial saturation of the π system,[4] by expansion of the π system through peripheral radial substitution with fused ring systems,[5] and by substitution of the *meso*-carbon atoms by aza nitrogen atoms or core modification by substitution of the pyrrole nitrogen atoms by oxygen, sulfur, and carbon.[6]

Until recently, research on the tetrabenzoporphyrins was substantially more limited in scope than is the case for porphyrins, porphyrazines, and phthalocyanines due to their low solubility arising from π–π stacking effects. Ono and co-workers developed the key breakthrough synthetic methodology for highly pure π-expanded porphyrinoids[7] and benzo[*c*] heterocyclic oligomers[8,9] based on tetramerization of pyrroles fused with bicyclo[2.2.2]octadiene (BCOD) to afford a peripherally substituted porphyrin, which can subsequently be converted to a tetrabenzoporphyrin in quantitative yield by heating at 200 °C.[10] A series of core-modified tetrabenzoporphyrins have recently been synthesized in which carbon, oxygen or sulfur atoms replace of one or both of the protonated pyrrole nitrogen atoms.[9,11] The compounds studied include the planar 21-carba- (**CN3**), 21-thia- (**SN3**), 21,23-dithia- (**S2N2**), and 21-oxa-23-thia- (**OSN2**) tetrabenzo[*b*,*g*,*l*,*q*]porphyrins reported previously by Ono and co-workers[11] as well as the previously unreported 21-oxa- (**ON3**) and 21-carba-23-thia- (**CSN2**) tetrabenzo-[*b*,*g*,*l*,*q*]porphyrins (Figure 1). The optical properties of these compounds are compared to those of tetrabenzo-[*b*,*g*,*l*,*q*]porphyrin (**TBP**), 5,10,15,20-tetraphenylporphyrin (**TPP**), 5,10,15,20-tetraphenyltetrabenzo[*b*,*g*,*l*,*q*]-21-thiaporphyrin (**TPSN3**), 5,10,15,20-tetraphenyltetrabenzo[*b*,*g*,*l*,*q*]-21,23-dithiaporphyrin (**TPS2N2**), 5,10,15,20-tetraphenyldibenzo[*g*,*q*]-21,23-dithiaporphyrin (**2BN**), 5,10,15,20 -tetraphenyldibenzo[*b*,*l*]-21,23-dithiaporphyrin (**2BS**), 5,10,15,20-tetraphenyltribenzo[*g*,*q*,*l*]-21-thiaporphyrin (**3BN**) and 5,10,15,20-tetraphenylbenzo[*b*]-21-thia-porphyrin (**1BS**) to examine the effect of ligand folding due to steric hindrance. The synthesis of monohetero- and diheteroporphyrins was pioneered by Ulman and Manassen in the mid-1970s.[12] The "thia" and "oxa" terminology for pyrrole nitrogen replacement within core-modified porphyrinoids, which was originally introduced by Johnson et al.,[13] is now well established in the literature,[6] despite the fact it would normally only be applied to replacement of a carbon atom.

Herein, we use a combination of magnetic circular dichroism (MCD) spectroscopy and theoretical calculations, specifically the time-dependent DFT (TD-DFT) and INDO/s techniques (INDO = intermediate neglect of differential overlap), to study the effect of core modification on the electronic structure and optical spectra of porphyrinoids. The effect of porphyrin-ring ligand folding is also investigated for compounds bearing phenyl groups at the *meso*-carbon atoms, since this has been the subject of considerable controversy in recent years.[14] The conformational flexibility of tetrapyrrolle macrocycles that is observed in protein crystal structures is believed to play a key role in determining the redox, spectroscopic, and catalytic properties of metalloenzymes. Sterically hindered porphyrins have been used as model compounds to study the effects of nonplanarity on the electronic structure. We recently reported an MCD spectroscopic study on tetraphenyltetraacenaphthoporphyrins (TPTANP),[15] which were reported by Lash et al.[5,16] to have the most red shifted B (or Soret) bands ever observed for porphyrinoids due to the effect of steric hindrance between the phenyl substituents and fused peripheral acenaphthalene rings. A set of anomalous negative Faraday $\mathcal{A}_1$ terms was observed in the MCD spectrum, due to reversal in the alignment of the magnetic moments of the optically accessible ππ* excited states owing to saddling of the ligand. A perimeter model approach was used to assign the optical spectra based on a D_{2d}-symmetric saddled structure derived from a B3LYP geometry optimization in which an S_4 symmetry axis is retained. The aim of this paper is to evaluate not only the effect of core modification but also the effect of the removal of the main C_4 or S_4 symmetry axis on the electronic structure of a series of planar and nonplanar core-modified free-base benzoporphyrins and to determine the extent to which the MCD technique can be used to test the accuracy of TD-DFT calculations and B3LYP optimized structures for nonplanar porphyrinoids and to continue our development[15] of tools which will allow us to move towards in silico design of novel porphyrinoids with specific properties based on theoretical predictions.

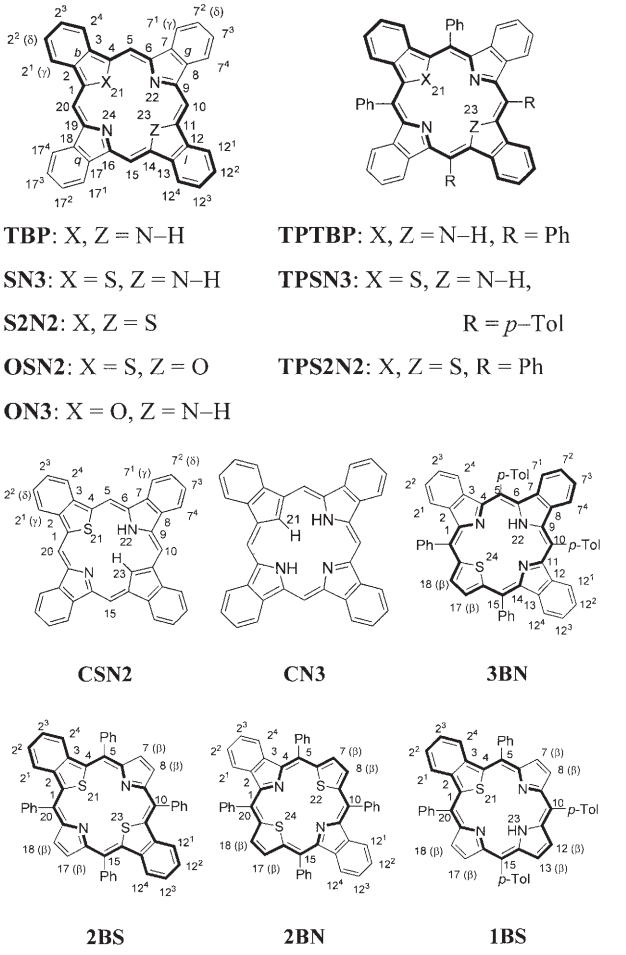

Figure 1. Structures of **TBP**, **SN3**, **S2N2**, **OSN2**, **ON3**, **TPTBP**, **TPSN3**, **TPS2N2**, **CSN2**, **CN3**, **3BN**, **2BS**, **2BN**, and **1BS** with carbon numbering schemes.[22] The pathway of the dominant ring current observed on the basis of NMR spectroscopy is shown in bold.

Results and Discussion

MCD spectroscopy of porphyrinoids: Many of the key breakthroughs in understanding the electronic structure of the porphyrinoids have been derived from MCD spectroscopy,[17] since the technique provides information on ground- and excited-state degeneracy that is required to fully assign the optical spectra of high-symmetry species. MCD spectra are recorded on a conventional CD spectrometer with a magnetic field applied parallel to the axis of light propagation (see the Supporting Information for more details). Analysis of MCD spectra is based on the Faraday $\mathscr{A}_1$, $\mathscr{B}_0$, and $\mathscr{C}_0$ terms due to Zeeman splitting of the absorption bands for left and right circularly polarized (lcp and rcp) light, the field-induced mixing of zero-field states, and the Zeeman splitting due to ground-state population adjustment, respectively (see Figures S1 and S2 in the Supporting Information). Since application of DFT techniques to properties based on magnetic dipole moment, such as MCD spectroscopy[18] has still to be fully developed, theoretical approaches based on semiempirical theoretical techniques such as Michl's perimeter model[19] and Gouterman's four-orbital model,[20] continue to play an important role in interpreting the optical spectra of porphyrinoids. Moffitt[21] and Michl[19] demonstrated that the electronic structures of heteroaromatic π systems can be described in terms of parent high-symmetry cyclic-polyene hydrocarbon perimeters, since the nodal patterns of the four frontier π MOs, which arise from the magnetic quantum number properties, are retained even after perturbations to the electronic structure. In the case of metal porphyrinoids, the orbital angular momentum (OAM) properties of the MOs which constitute the π system can be described in terms of an $M_L = 0, \pm1, \pm2, \pm3, \pm4, \pm5, \pm6, \pm7$, 8 sequence in ascending energy, associated with the D_{16h}-symmetric $C_{16}H_{16}^{2-}$ parent perimeter for the 18 π electrons on the 16-atom inner ligand perimeter, since the four pyrrole nitrogen atoms have identical partial charges. In the case of free-base porphyrinoids, however, the parent perimeter is usually viewed as being $C_{18}H_{18}$ with the MOs arranged in an $M_L = 0, \pm1, \pm2, \pm3, \pm4, \pm5, \pm6, \pm7, \pm8$, 9 sequence, since the $2p_z$ atomic orbitals of the protonated pyrroles contain a lone pair of electrons. In the context of Gouterman's four-orbital model,[20] the optical spectroscopy is based on an allowed transition to the B state ("$\Delta M_L = \pm1$") arising from the Ψ_{-4}^{-5} and Ψ_4^5 excited-state configurations and a forbidden transition to the Q state ("$\Delta M_L = \pm9$") arising from the Ψ_4^{-5} and Ψ_{-4}^5 excited-state configurations, which arise from the four spin-allowed transitions linking the HOMOs ($M_L = \pm4$) and the LUMOs ($M_L = \pm5$); see Figure 2 and Figure S3 in the Supporting Information. Within Michl's perimeter model[19] the induced excited-state magnetic moments of these ideal B and Q states are referred to as μ^- and μ^+, respectively.

Michl[19] predicted, based on an LCAO approach to the perimeter model, that the magnetic moments associated with the B and Q bands (μ^- and μ^+) of a $C_{16}H_{16}^{2-}$ parent perimeter are -0.01 and -6.24β, respectively, while the corresponding values for a $C_{18}H_{18}$ perimeter are -0.36 and -6.83β. Under ideal D_{16h} or D_{18h} symmetry, the Q_{00} band is fully electric dipole forbidden and can gain intensity only through vibrational borrowing from the allowed B_{00} band.

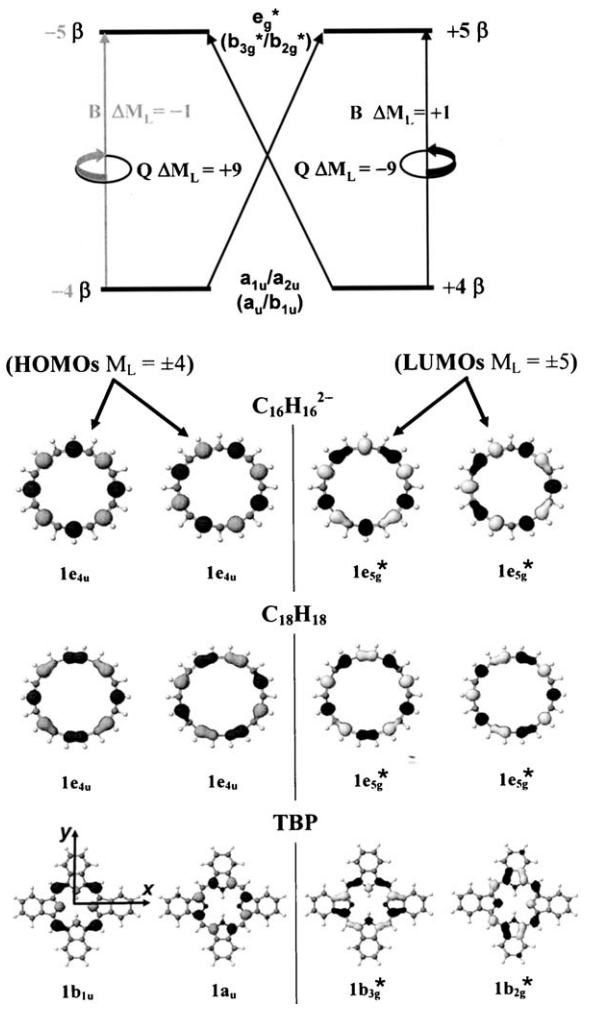

Figure 2. Top: Origin of the Q and B bands in Gouterman's four-orbital model.[20] In the context of a free-electron model, the doubly degenerate HOMO and LUMO of the inner cyclic polyene perimeter exhibit ±4 and ±5 β of angular momentum, respectively. The four possible spin-allowed transitions result in the forbidden "Q" band with "$\Delta M_L = \pm9\,\beta$" and the allowed "B" band with "$\Delta M_L = \pm1\,\beta$". These bands are readily recognized in the absorption and MCD spectra of most main group metal and free-base porphyrinoids. The symmetries of the real MOs arising from these complex MOs are shown for the D_{4h} symmetry of metal porphyrinoid complexes and the typical D_{2h} symmetry of free-base porphyrinoids (in parentheses). When the symmetry is reduced to D_{2h}, the zero-field splitting of the excited states that is introduced splits the Q and B bands into their *x*- and *y*-polarized components. Bottom: The four frontier π MOs of the $C_{16}H_{16}^{2-}$ and $C_{18}H_{18}$ parent perimeters and **TBP** from INDO/s calculations generated using the CAChe workstation software package at the 0.04 a.u. energy level of the isosurface value for electrostatic potential exhibit the $M_L = \pm4$ and $M_L = \pm5$ nodal patterns anticipated on the basis of Gouterman's four-orbital model[20] and Michl's perimeter model.[19] The nodal patterns for all of the compounds in Figure 1, generated from Gaussian checkpoint files[41] for TD-DFT calculations using CS Chem 3D and from INDO/s calculations using the CAChe workstation software package,[42] are provided as Figure S3 in the Supporting Information.

The sign and intensity of the $\mathscr{A}_1$ term arising from the B transition is determined only by the far weaker μ^- moment. In the case of D_{4h}- and D_{2h}-symmetric cyclic perimeters, there is mixing of the allowed and forbidden character of the B and Q transitions, and the B and Q excited states acquire both μ^- and μ^+ character. The μ^- contribution tends to be largely independent of structural changes, whereas the μ^+ contribution can change sign depending on the nature of the perturbations to the structure of the perimeter. The degree of mixing α and the magnitude of the induced magnetic dipoles μ(B) and μ(Q) associated with the B and Q excited states can be estimated by using Michl's perimeter model,[19] based on the observed dipole strengths $\mathscr{D}_0$ [Eqs. (1)–(3)].

$$\mathscr{D}_0(\mathrm{Q})/\mathscr{D}_0(\mathrm{B}) = \tan^2\alpha \quad (1)$$

$$\mu(\mathrm{B}) = \pm(\cos^2\alpha)\mu^- \pm (\sin^2\alpha)\mu^+ \quad (2)$$

$$\mu(\mathrm{Q}) = \pm(\sin^2\alpha)\mu^- \pm (\cos^2\alpha)\mu^+ \quad (3)$$

Michl[19] demonstrated that in the case of lower symmetry chromophores, such as the core-modified TBPs in this study, in which complete lifting of the orbital degeneracies of the four frontier π MOs occurs (Figure 2) the alignment of the induced magnetic moments with and against the axis of light propagation and the applied field (and hence the ordering of the signs for the Q_x, Q_y, B_x, B_y MCD spectral bands), based on the μ^+ moment contribution, can be determined by the relative magnitude of the splitting of the HOMOs and the LUMOs of the parent perimeter (ΔHOMO and ΔLUMO), since this determines whether the circulation of electronic charge in the LUMOs or that of the hole left in the HOMOs is the dominant factor in conserving the quantum of OAM provided by the incident photon of left or right circularly polarized light. When ΔHOMO > ΔLUMO, electronic charge circulation in the LUMO predominates and the ordering of the negative and positive Faraday $\mathscr{B}_0$ terms arising from the Q and B transitions, due to the differential absorbance of lcp and rcp on which MCD intensity is based, is −, +, −, + in ascending energy terms (analogous to two positive derivative-shaped $\mathscr{A}_1$ terms). In contrast, when ΔLUMO > ΔHOMO the positive charge associated with the hole left in the HOMO is the predominant factor and the sequence reverses to +, −, +, − (analogous to two negative derivative-shaped $\mathscr{A}_1$ terms), as has been observed previously in the MCD spectra of the chlorins, where ΔLUMO > ΔHOMO due to the effect of the reduction of the porphyrin π system at the ligand periphery.[20]

In summary, changes in symmetry will reduce the OAM associated with both the doubly degenerate HOMO and LUMO of the π system of the parent cyclic-polyene hydrocarbon perimeter, but the nodal patterns associated with the magnetic quantum number properties are still retained.[19] The anomalous +, −, +, − sign sequence is observed when perturbations to the structure quench the OAM of the two LUMOs to a greater extent than the two HOMOs.

Optical spectroscopy: The UV/Vis absorption and MCD spectra of **TPP**, **TBP**, **SN3**, **ON3**, **S2N2**, **OSN2**, **TPSN3**, **TPS2N2**, **1BS**, **3BN**, **2BN**, **2BS**, **CN3**, and **CSN2** are shown in Figure 3. As reported previously by Ono and co-workers[9,10] in the case of **SN3**, **S2N2**, and **OSN2**, the spectra of the near-planar **ON3**, **SN3**, **S2N2**, and **OSN2** are similar to those of **TBP** with only minor shifts of the band centers of the main Q and B bands. Intensity in the UV region increases and the B bands become less intense when a pyrrole NH group is replaced by an O or S atom. In the case of **CN3** and **CSN2** the changes are more pronounced. In the visible region, the presence of intense pseudo-Faraday $\mathscr{A}_1$ terms in the MCD spectrum indicates that the zero-field splitting of the Q bands is small. However, splitting of the B bands is marked, and the higher energy bands in the UV region gain significant intensity. The Q and B bands of **TPSN3** and **TPS2N2** exhibit a marked redshift, while the Q_{00} bands are significantly less intense and the Q_{x0} and Q_{y0} bands less resolved relative to **SN3** and **S2N2**. In the case of the nine non-phenylated compounds the sign sequence of the Q_{00} and B_{00} bands is −, +, −, + in ascending energy terms, as is typically observed for most porphyrinoids.[15,17] Despite the effect of ligand folding, core substitution with heteroatoms and partial benzo substitution, the additional information on band polarization derived from the sign sequences in the MCD spectra makes it clear that the optical spectra of **2BN** and **3BN** are similar to that of **TPP**, since the sign sequence in the Q-band region is −, −, +, +, and a pseudo-$\mathscr{A}_1$ term in the B-band region has a −, + sign sequence. The degree of separation of the Q_{x0} and Q_{y0} bands is clearly greater than that of the Q_{x0} and Q_{x1} bands. In the case of **1BS** and **2BS**, the sign sequence of the Q_{00} bands is reversed, and an anomalous +, −, −, + sequence for the main Q_{00} and B_{00} bands results.

Geometry optimizations: The B3LYP optimized geometries are shown in Figure 4. With the exception of **TPP**, the tetraphenyl-substituted complexes are predicted to be nonplanar due to steric hindrance between the phenyl groups on the *meso*-carbon atoms and peripheral fused benzene rings. Compounds **1BS** and **2BN** are nearly planar, however, due to the effect of partial benzo substitution. Whereas **TBP**, **SN3**, **ON3**, **S2N2**, and **OSN2** are planar, core substitution with a carbon atom to form **CN3** and **CSN2** also results in a nonplanar structure. In the case of the 21,23-diheteroporphyrins, incorporation of two O and/or S atoms to replace pyrrole NH results in marked distortion of the geometry of the inner perimeter of the π system. A less pronounced effect is observed in the 21-heteroporphyrin structures.

X-ray structural analysis: We conducted X-ray analyses to investigate the relationship between the molecular structures and optical spectra of core-modified tetrabenzoporphyrins (Figure 5). Suitable single crystals could only be obtained for **TPS2N2**·1.5 $CHCl_3$, **TPSN3**·1.5 $CHCl_3$, **3BN**·3 $CHCl_3$, **2BS**, **2BN**, and **1BS** due to the low solubility of the non-phenylated compounds. In the crystal of

TPSN3·1.5 $CHCl_3$, the **TPSN3** molecule is disordered. The less common structure (12.5%) occupies the same position as the main structure (87.5%), but the porphyrin plane is rotated by 90°. Only the core heteroatoms of the less common structure could be refined. In the case of **2BS** and **2BN**, the porphyrin molecules occupy special positions and adopt a wave out-of-plane distortion. The results are summarized in the Experimental Section. Edge views are shown in Figure 5. In a similar manner to **TBTBP**,[22] peripheral expansion of the π system with fused benzene rings results in severe saddling in the case of **TPS2N2**, **TPSN3**, and **3BN**: the plane angles of opposite indole and isothianaphthene moieties were 131.56(6) and 134.40(5)° in **TPS2N2**, 128.70(7) and 138.00(4)° in **TPSN3**, and 136.68(6) and 143.62(7)° in **3BN**. The most striking feature is the distortion of the benzo rings observed in the isothianaphthene moieties of **2BS**. The angle between the planes of the five thiophene atoms and four benzo carbon atoms is 9.86(7)°. The largest discrepancy between experimental and calculated structures is observed in **TPSN3** (Figures 4 and 5), as would be anticipated based on the fact that the **TPSN3** molecules are disordered in the crystal structure. The other minor differences are probably due to crystal packing effects and are not necessarily present in solution.

Cyclic and differential pulse voltammetry: CV and DPV measurements were carried out for all of the compounds, but oxidation and reduction potentials could only be derived for **TPS2N2**, **TPSN3**, **1BS**, **2BS**, **2BN**, and **3BN** due to low solubility of the non-phenylated compounds (see Figure S4 in the Supporting Information). As anticipated, the separations of the first oxidation and reduction potentials are similar to the Q band energies (see Figure S5 in the Supporting Information).

NMR spectroscopy: ^{1}H NMR studies, including differential NOE experiments, were carried out for **TPS2N2**, **TPSN3**, **1BS**, **2BS**, **2BN**, and **3BN**. No NMR measurements could be made for the non-phenylated compounds due to their low solubility. The most distinctive feature of the ^{1}H NMR spectra of **TPS2N2**, **TPSN3**, **1BS**, **2BS**, **2BN**, and **3BN** is that the signals of the benzo protons of the isoindole moieties lie at higher field than the corresponding isothianaphthene protons (see data reported in the Experimental Section, and Figure 1 for carbon numbering). The signals for isoindole γ protons that are adjacent to a thiophene and isothianaphthene moieties, such as $H7^1$ (**TPS2N2**, **TPSN3**), $H7^4$ (**TPS2N2**, **TPSN3**), $H2^1$ (**3BN**), and $H2^4$ (**3BN**), appear at higher field than the corresponding δ protons such as $H7^2$ (**TPS2N2**, **TPSN3**), $H7^3$ (**TPS2N2**, **TPSN3**), $H2^2$ (**3BN**), and $H2^4$ (**3BN**) due to the anisotropic shielding effect of the aryl groups, whereas the signals for isoindole γ protons that are opposite to the thiophene and isothianaphthene moieties, such as $H12^1$ (**TPSN3**), $H12^4$ (**TPSN3**), $H7^1$ (**3BN**), and $H7^4$ (**3BN**), were observed at similar or slightly lower field than those of the corresponding δ protons.

The signals for the benzo protons of **TPSN3** lie at higher field than the corresponding signals in the spectrum of **1BS** due to a strong shielding effect when the *meso*-phenyl groups are fixed in positions that are orthogonal to the macrocyclic planes by steric interaction with two adjacent benzo moieties. In the cases of **2BS** and **2BN**, the shielding effect of the phenyl groups is also thought to be smaller since they can rotate more freely. The ^{1}H NMR spectrum of **3BN** is highly complex but can be rationalized by careful consideration of the above effects. In the case of **TPS2N2**, the proton signals of isoindole moieties were observed at $\delta =$ 7.17 (δ positions: $H7^2$, $H7^3$, $H17^2$, and $H17^3$) and 6.89 ppm (γ positions: $H7^1$, $H7^4$, $H17^1$, and $H17^4$), whereas the signals due to isothianaphthene moieties appeared at $\delta = 7.83$ (γ positions) and 7.35 ppm (δ positions). Similarly, benzo proton signals for **2BN** ($\delta = 7.37$ and 7.20 ppm) appeared at higher field than for **2BS** ($\delta = 8.05$ and 7.59 ppm), whereas the β-proton signals in the spectrum of **2BN** ($\delta = 9.34$ ppm) were observed at lower field than in the case of **2BS** (8.33 ppm). As benzo protons of the parent heterocycles exhibit similar chemical shifts ($\delta = 7.5$ and 6.8 for isoindole and $\delta = 7.59$ and 7.04 for isothianaphthene),[23] these observed differences can be attributed to differences in the diamagnetic macrocyclic ring currents (Figure 1).

In all cases, considerable anisotropic downfield shifts were observed due to the enlarged macrocyclic π systems, not only in the case of the *ortho* but also for the *meta* and *para* proton signals of the *meso*-aryl groups. Similar NMR data were reported previously for tetraphenyltetrabenzoporphyrin.[24] In the ^{1}H NMR spectra of **TPSN3** and **TPS2N2**, in which the phenyl groups sit between two benzo moieties, the *ortho* signals lie at $\delta = 8.33$–8.27 ppm, and the other phenyl proton signals at $\delta = 7.92$–7.87 ppm.

In the case of **1BS**, **2BS**, **2BN**, and **3BN**, the phenyl groups of which are adjacent to only one benzo moiety, the resonances appeared at slightly higher field (*ortho*: $\delta = 8.25$–8.05, *meta* and *para*: $\delta = 7.87$–7.79 ppm). A similar trend was observed in the shifts of the *p*-tolyl groups. In contrast to the *meso*-aryl protons, the signals of the benzo protons generally appear at higher fields compared to *meso*-unsubstituted benzoporphyrins.[10b] Cheng and co-workers[25] used variable-temperature (VT) NMR experiments to study the dynamic behavior of free-base **TPTBP**. They suggested that the temperature effect observed in the ^{1}H NMR spectrum was not only due to inner proton tautomerism but also to effects related to conformational change of the saddle-shaped macrocycle and the restricted movement of the phenyl groups. However, they were unable to assign the low-temperature spectra.

We recorded VT NMR spectra of free-base **TPTBP** (Figure 6). Based on analysis of the ^{1}H NMR spectra of **TPTBP** in $CDCl_3$ at 20 °C, the benzo protons can be assigned to the very broad signal observed at $\delta = 7.25$ ppm. This signal is resolved at 50 °C into two multiplets at $\delta = 7.18$ and 7.23 ppm. Owing to the low boiling point of $CDCl_3$, the solvent was changed to [D_6]DMSO for higher temperature measurements. The multiplets for an AA′BB′ spin system

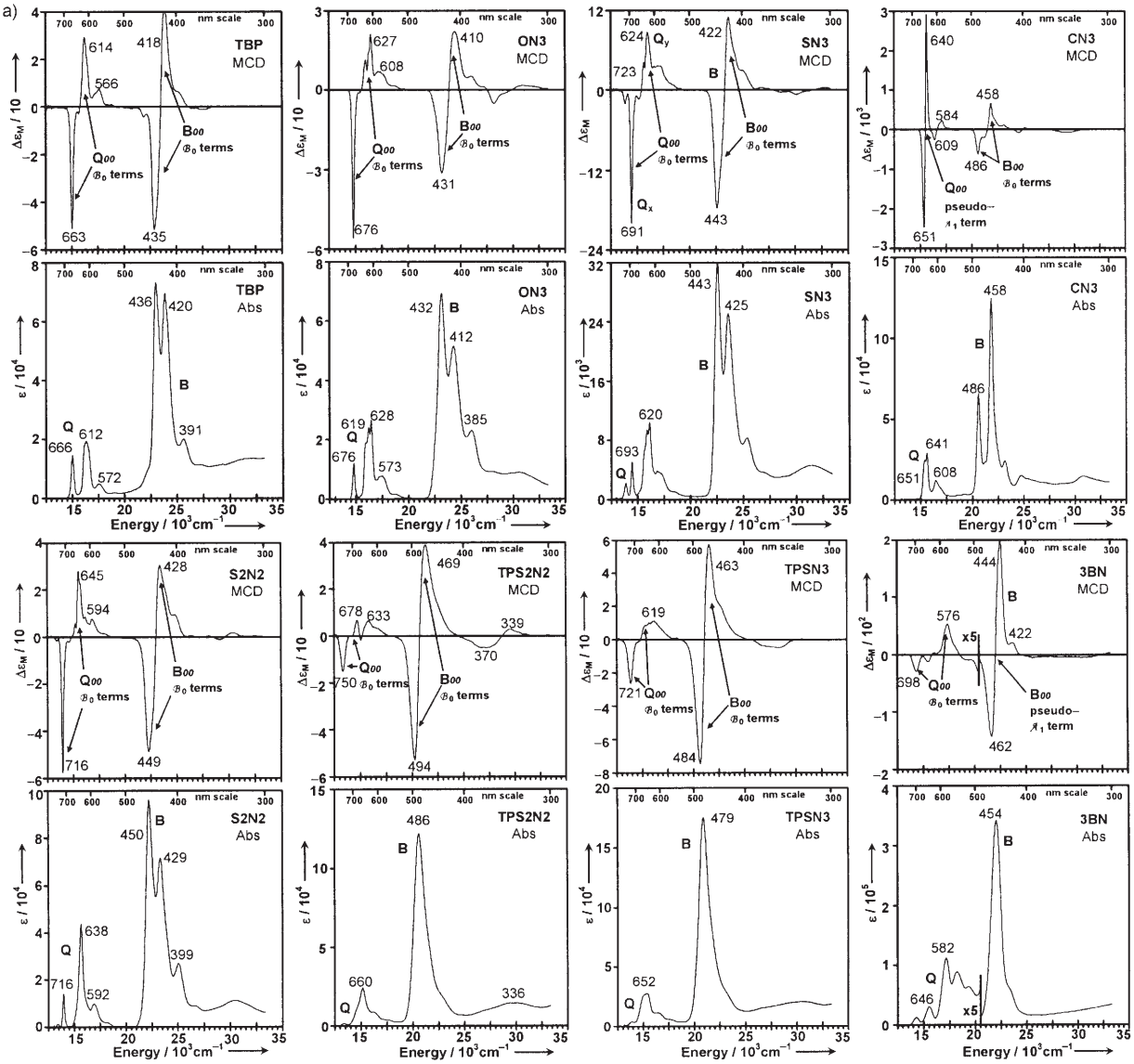

Figure 3. a) UV/Vis absorption and MCD spectra of **TBP**, **ON3**, **SN3**, **CN3**, **S2N2**, **TPS2N2**, **TPSN3**, **3BN** in DMF at 298 K. The spectra of the planar compounds core-modified with S or O atoms are similar to those of **TBP**, while the spectra of **CN3** and **CSN2** are markedly different. An anomalous +/− MCD sign sequence is observed in the Q-band region of **1BS** and **2BS** but not in that of **TPS2N2**, **TPSN3**, **2BN**, and **3BN**. The spectra of **2BN** and **TPP** are very similar despite the markedly different molecular structures, since $\Delta HOMO \approx \Delta LUMO$, as is shown in Figure 8 below. b) UV/Vis absorption and MCD spectra of **1BS**, **2BS**, **2BN**, **H_2TPP**, **OSN2**, **CSN2**, H_2OEP, and $[H_4OEP]^{2+}$ in DMF at 298 K. The spectra of the planar compounds core-modified with S or O atoms are similar to those of **TBP**, while the spectra of **CN3** and **CSN2** are markedly different. An anomalous +/− MCD sign sequence is observed in the Q-band region of **1BS** and **2BS** but not in that of **TPS2N2**, **TPSN3**, **2BN** and **3BN**. The spectra of **2BN** and **TPP** are very similar despite the markedly different molecular structures, since $\Delta HOMO \approx \Delta LUMO$, as is shown in Figure 8 below.

observed at $\delta = 7.14$ and 7.27 ppm can be unambiguously assigned as arising from the γ and δ protons, respectively. The low-temperature NMR spectra are rather complicated, as Cheng et al. reported.[25] The broad singlet at 20 °C is resolved into three broad signals at 0 °C, the lowest of which is further resolved into two signals below −10 °C. At −50 °C, the two pairs of the AA′BB′ spin systems can be clearly observed, and all the signals can be assigned by comparison with the spectra of **TPSN3** (see Experimental Section). The AA′BB′ multiplets arising from the 2*H*-isoindole moieties lie at $\delta = 7.35$ (δ protons: $H2^2$, $H2^3$, $H12^2$, and $H12^3$) and 7.43 ppm (γ protons: $H2^1$, $H2^4$, $H12^1$ and $H12^4$), while the AA′BB′ protons of isoindolenine (1*H*-isoindole) moieties absorb at higher fields: $\delta = 6.99$ (γ protons: $H7^1$, $H7^4$, $H17^1$,and $H17^4$) and 7.18 ppm (δ protons: $H7^2$, $H7^3$, $H17^2$ and $H17^3$). The coalescence at 20 °C can be ascribed to inner pyrrolic proton tautomerism. No evidence for other dynamic effects, such as macrocyclic ring inversion, is observed. Lash et al.[5] have reported similar results for TPTANP.

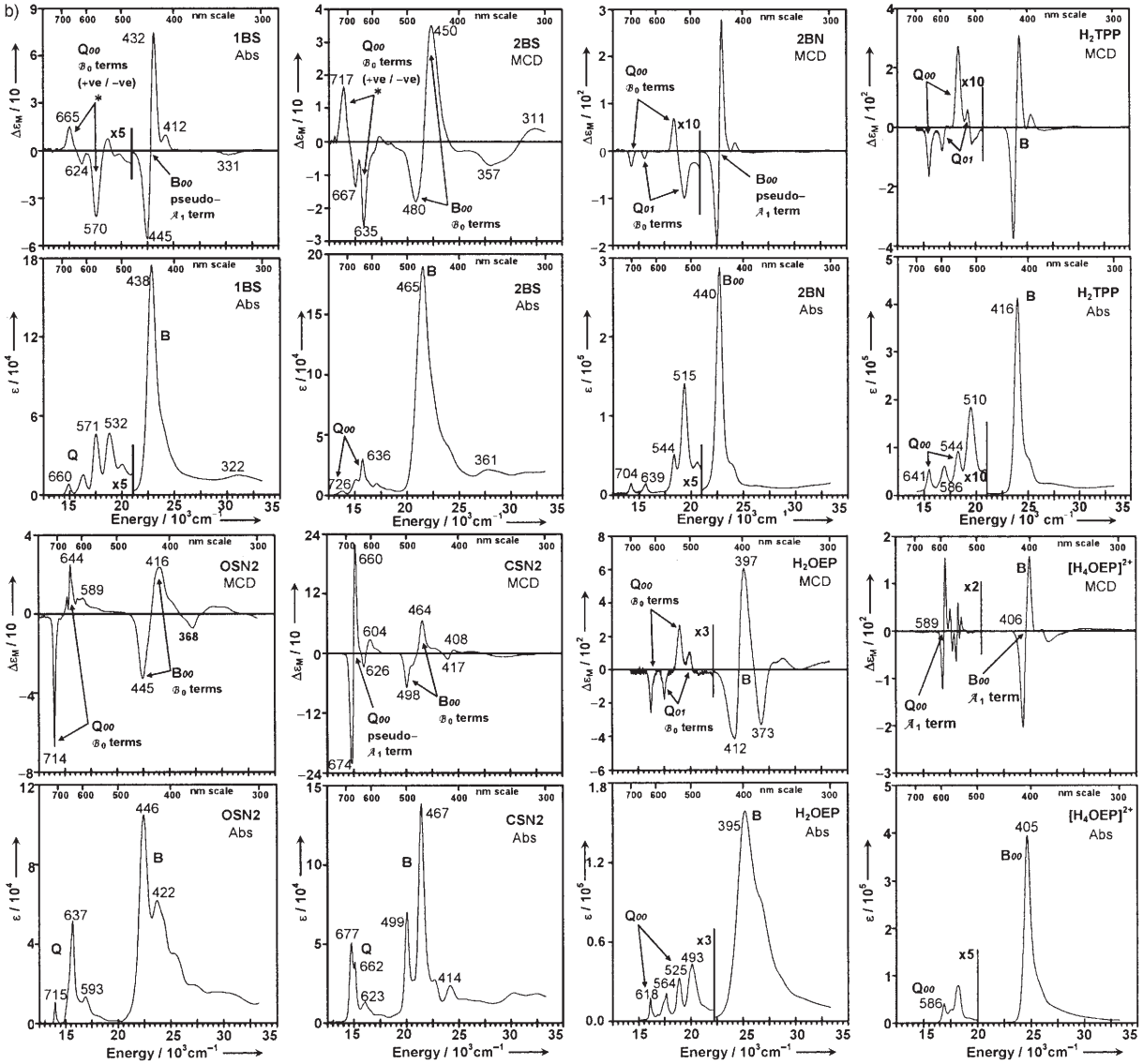

Figure 3 (continued).

Discussion

The electronic and optical properties of a large number of core-modified tetrabenzoporphyrins were analyzed to investigate the relative effects of core modification of pyrrole N with C, S, and/or O atoms, ligand folding, and partial benzo substitution on the electronic structure and optical properties. We have shown previously in our recent analysis of TD-DFT and INDO/s calculations derived from the B3LYP geometry optimizations of ZnTPTANP and 16 other radially symmetric Zn^{II} porphyrinoids[15] that the peripheral structure and overall symmetry of porphyrinoids has a systematic effect on the energies and oscillator strengths of the Q and B bands and the OAM properties of the associated excited states. Our analysis pointed to the accidental degeneracy of the two frontier π MOs derived from the e_{4g} HOMO of the $C_{16}H_{16}^{2-}$ parent perimeter and an orbitally degenerate 1e* LUMO due to saddled D_{2d} symmetry being responsible for the unusually large redshift of the B (or Soret) band.[15] When $\Delta HOMO \approx \Delta LUMO \approx 0$, the electronic structure mimics that of a high-symmetry $C_{16}H_{16}^{2-}$ perimeter. The anomalous MCD spectrum can be accounted for on this basis, since the alignments of the induced ππ* excited-state magnetic dipoles in π systems of this type are known to be sensitive to minor structural perturbations when the Q band is fully forbidden and the weaker μ^- moment predominates.

The methods used to analyze the trends observed in the data in that study[15] can also be applied here. Indeed, the new data compliment and add to those previous data. We discuss each of the sets of compounds individually below. What was not clear during the analysis of the MCD spectrum of ZnTPTANP was the extent to which nonplanarity affects the MCD spectra of lower symmetry porphyrinoid π systems in which $\Delta HOMO \neq \Delta LUMO \neq 0$, where the larger

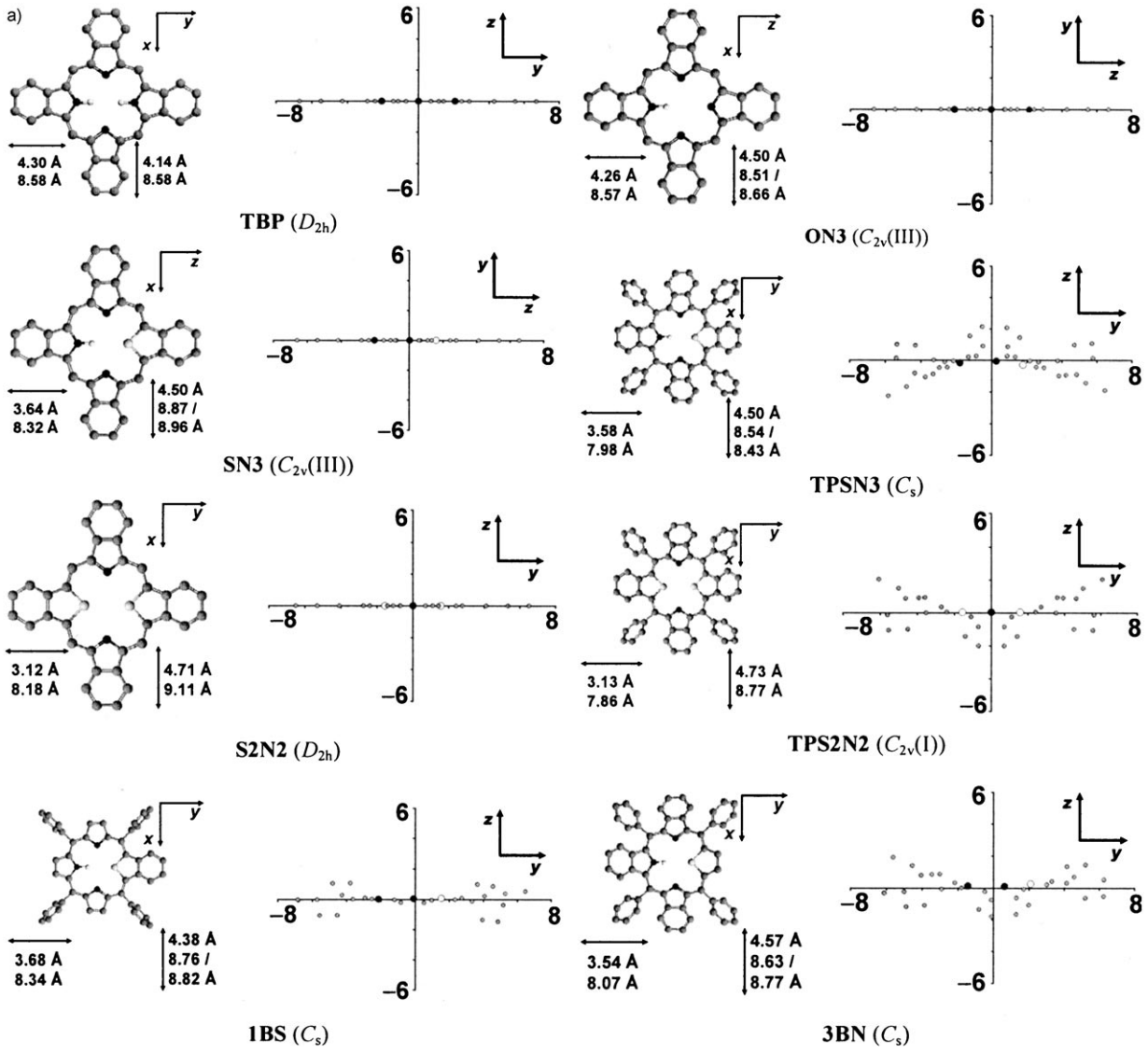

Figure 4. a) B3LYP-optimized geometries of **TBP**, **ON3**, **SN3**, **TPSN3**, **S2N2**, **TPS2N2**, **1BS**, and **3BN**, with a cross-section view provided to show the deviation [Å] from ligand planarity. The axes are rotated clockwise by 90° relative to the structures in Figures 1, 2, 11, and Figure S3 in the Supporting Information in all cases so that the heteroatoms are more clearly visible. In the case of **SN3** and **ON3**, the *y* and *z* axes are switched relative to the axes used for **TBP** and the other compounds, since the main twofold axis of symmetry lies in the plane of the π system. The distance between opposite pyrrole N (or S, O, and/or C) atoms and the distance between opposite β-carbon atoms is provided to illustrate the effect of core substitution on the geometry of the central cavity. b) B3LYP optimized geometries of **2BN**, **2BS**, **OSN2**, **CSN2**, **TPTBP**, and **CN3** with a cross-sectional view showing the deviation [Å] from ligand planarity. The axes are rotated clockwise by 90° relative to the structures in Figures 1, 2, 11 and Figure S3 in the Supporting Information in all cases except **CN3** and **CSN2** so that the heteroatoms are more clearly visible. In the case of **OSN2**, the *y* and *z* axes are switched relative to the axes used for **TBP** and the other compounds, since the main twofold axis of symmetry lies in the plane of the π system. The distance between opposite pyrrole N (or S, O, and/or C) atoms and the distance between opposite β-carbon atoms is provided to illustrate the effect of core substitution on the geometry of the central cavity.

μ^+ contribution to the excited-state magnetic moments can be expected to become a much more significant factor. Unlike phthalocyanines where $\Delta HOMO \gg \Delta LUMO$, the spectra of TBPs remain reasonably similar to those of the porphyrins,[19] and the observed α value based on the dipole strengths of the Q and B bands [Eqs. (1)–(3)], is low enough that the effect of introducing a significant ΔLUMO through demetalation creates a chromophore that is potentially susceptible to MCD sign reversal. We analyzed the MCD spectra to determine trends in the band energies, intensities, and signs to test the validity of the TD-DFT and INDO/s calculations of core-modified tetrabenzoporphyrins (Figures 7–13, Table 1 and Tables S1–S3 in the Supporting Information), similar to the approach we adopted with radially symmetric zinc porphyrinoids.[15] The trends observed in calculations based on the six crystal structures (Figure 5) are very similar to those observed in the B3LYP calculations (Figures 9 and 11, Table 1 and Table S1 in the Supporting Information), so our analysis focused primarily on the latter.

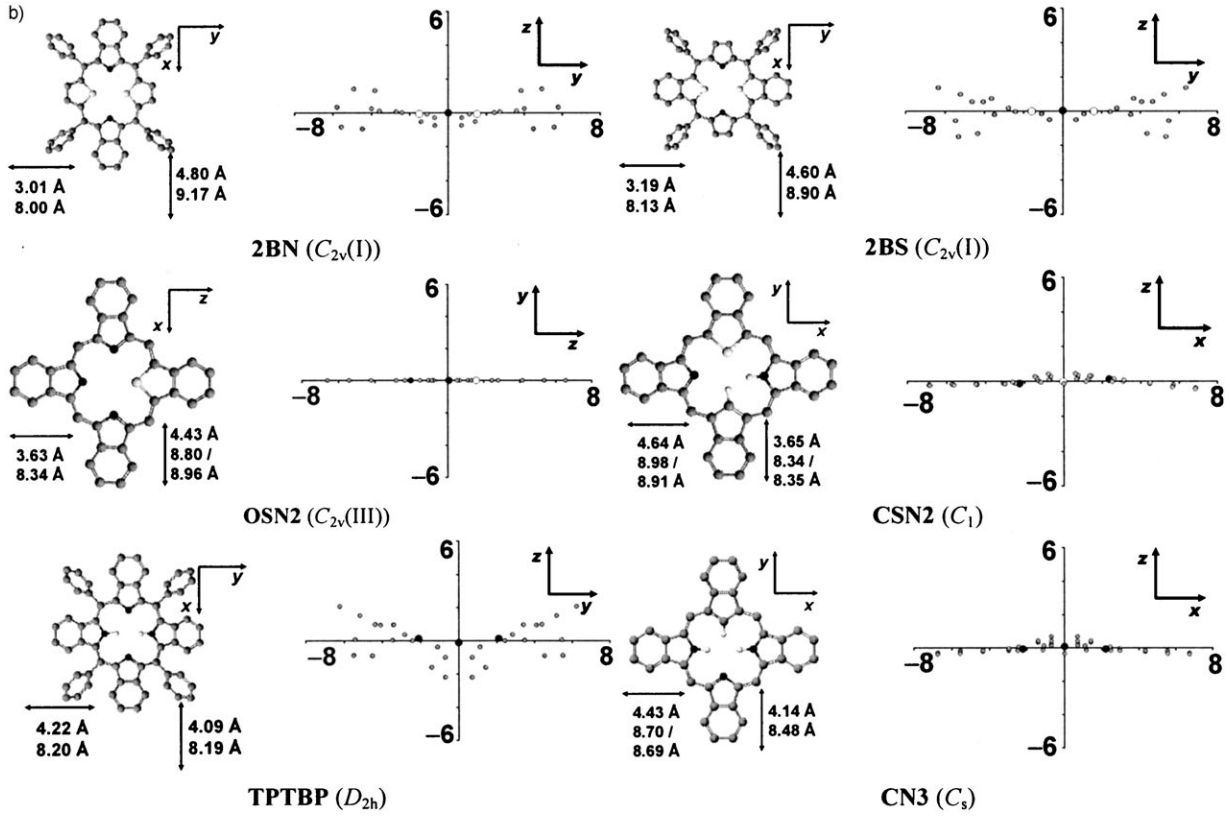

Figure 4 (continued).

When the ΔHOMO and ΔLUMO values predicted on the basis of TD-DFT and INDO/s calculations for **TBP**, **S2N2**, **SN3**, **1BS**, **2BS**, **2BN**, and **3BN** the parent monobenzo[*b*]-, adj-dibenzo[*b*,*g*]-, opp-dibenzo[*b*,*l*]-, tribenzo-[*b*,*g*,*l*]porphyrins and their 5,10,15,20-tetraphenyl analogues, as well as the non-phenylated analogues of **1BS**, **2BS**, **2BN** and **3BN** are plotted (Figure 10), the two major trends that are observed are a decrease in the ΔHOMO values on phenylation and a slight increase in ΔLUMO due to core modification with O and/or S atoms. These predictions are consistent with the observed spectral data, since the Q bands of **TPSN3** and **TPS2N2** are considerably less intense than those of **SN3** and **S2N2** [Eqs. (1)–(3) and Figures 3 and 9], and a slightly greater splitting of the *x*- and *y*-polarized components of the symmetry-split Q and B bands can be observed in the case of **ON3**, **SN3**, **S2N2**,and **SON2** (Figures 3 and 11). Partial benzo substitution is predicted to have a significantly greater effect than the other structural modifications, since the core-modified compounds lie closer to the parent porphyrins and benzoporphyrins than to each other (Figure 10). Although a slight stabilization of the frontier π-MOs corresponding to the $1b_{3g}$* MO of **TBP** is predicted in the case of **S2N2** and **OSN2** relative to **SN3** and **ON3**, and in turn relative to **TBP** (Figure 11; significant MO coefficients are predicted for the N, S, and/or O atoms at the 21- and 23-positions; see Figure 1, Figure 12, and Figure S3 in the Supporting Information), the changes observed in the optical spectra (Figures Figures 3 and 11) and in the OAM properties of the π system (Figure 2, Figure 12 and Figure S3 in the Supporting Information) on core modification with O and S atoms are relatively minor, since the lone pair of electrons in the $2p_z$ atomic orbital (AO) of the N atom in the pyrrole NH group is directly replaced by another lone pair of electrons in the $2p_z$ or $3p_z$ AOs of the O or S atom (Figure 1). In the case of core modification with C and S atoms to form **CSN2**, however, significantly greater effects are observed (Figures 2, 3, 4, 11 and Figure S3 in the Supporting Information, since a pyrrole nitrogen atom is protonated on the *x* axis to compensate for the fact that the $2p_z$ AO of the carbon atom does not contain a lone pair. This substantially alters the geometry of the 18-atom perimeter since it involves the β-carbon atoms on adjacent pyrrole moieties due to the two lone pairs on the inner π system perimeter being located on adjacent rather than opposite heteroatoms (Figure 1). The Q bands of **CSN2** form an intense pseudo-$\mathscr{A}_1$ term (Figure 3 and Figure S2 in the Supporting Information), since the effect of the structural perturbation arising from the adjacent lone pairs is identical along the *x* and *y* axes of the parent perimeter. Although the fact that the spectra of **CN3** and **CSN2** are almost identical would appear to point to the structure with adjacent lone pairs being the more stable tautomer in the case of **CN3** as well, the TD-DFT calculations of the opposite and adjacent **CN3** tautomers are very similar (Figure 11).

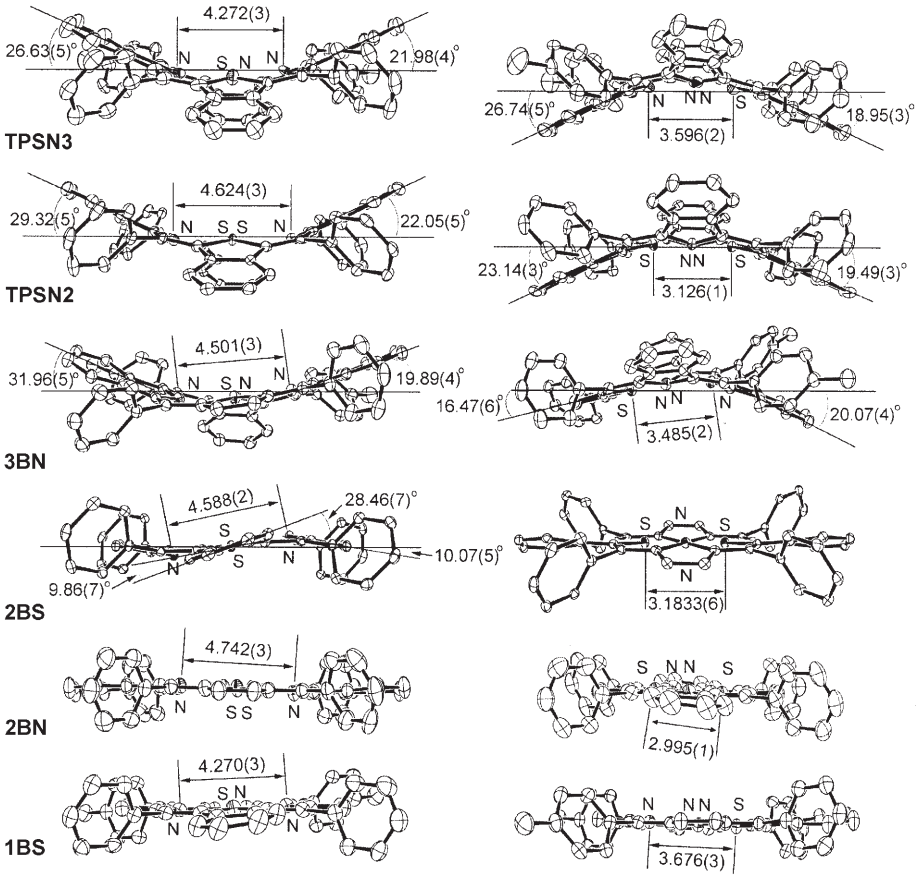

Figure 5. Edge views of ORTEP drawings of **TPSN3**, **TPS2N2**, **3BN**, **2BS**, **2BN**, and **1BS**. Left: views along opposite nitrogen atoms. Right: views along opposite heteroatoms.

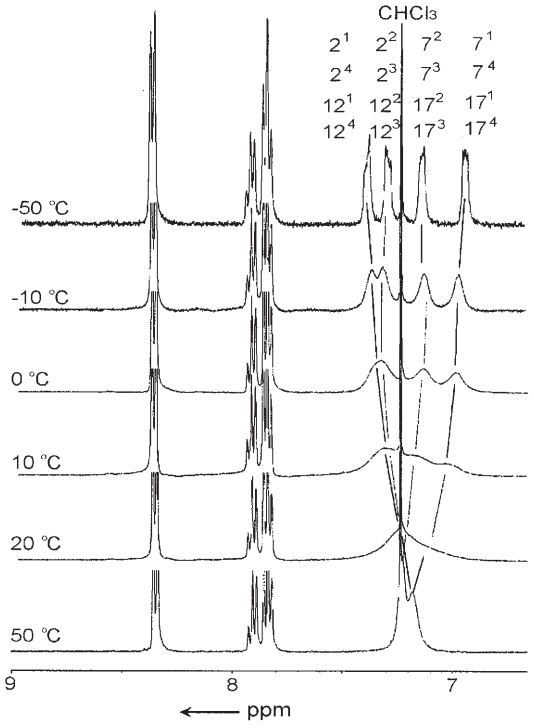

Figure 6. Variable-temperature NMR spectra of **TPTBP** in $CDCl_3$.

The UV/Vis absorption spectrum of **2BN** is markedly different from that of **2BS** despite the similar structures (Figure 3). Note that a somewhat similar absorption spectrum to that of **2BN** was reported by Clezy et al.[26] for the parent non-core-modified dibenzo[*b*,*q*]porphyrin compound, so this is probably related primarily to the fused-ring substitution pattern rather than core modification. The weak absorption bands at 639 and 704 nm are sufficiently separated from the bands at 515 and 544 nm that their assignment would be problematic in the absence of MCD spectral data. Both these bands appear as negative $\mathscr{B}_0$ terms in the MCD spectrum, as opposed to the normal pattern of a coupled pair of oppositely signed bands. This is clear evidence that the spectrum is similar to that of **TPP** despite core modification and partial benzo substitution. The observed spectral pattern can be readily explained by adopting a perimeter-model approach. The optical spectra of free-base porphyrinoids are best described in terms of a perturbed $C_{18}H_{18}$ parent perimeter (Figure 2) due to the lone pairs associated with the two protonated pyrrole nitrogen atoms rather than the $C_{16}H_{16}^{2-}$ perimeter of metal complexes, where there are no protonated pyrrole nitrogen atoms, or the $C_{20}H_{20}^{2+}$ perimeter of porphyrin dications, where there are four. This leads to marked spectral changes, as can be observed in the spectra of H_2OEP and $[H_4OEP]^{2+}$ (Figure 2). The MCD spectrum of $[H_4OEP]^{2+}$ is dominated by derivative-shaped Faraday $\mathscr{A}_1$ terms, since the excited states are orbitally degenerate, while the Q-band region of H_2OEP is comprised of Gaussian-shaped Faraday $\mathscr{B}_0$ terms due to the absence of a threefold, or higher, axis of symmetry.[17] A key feature of $D_{(4N+2)h}$ ($N>1$) symmetry is that the multiplication products of the LUMO and HOMO symmetries are both singly and doubly degenerate (for the e_{1u} and e_{2u} MOs in the D_{6h} symmetry of benzene the product is e_{1u}, b_{1u}, and b_{2u}), whereas in $D_{(4N)h}$ ($N>1$) symmetry the multiplication products are only doubly degenerate (for the e_{4u} and e_{5u} MOs in the D_{16h} symmetry of $C_{16}H_{16}^{2-}$ the product is e_{1u} and e_{7u}). Although the B bands form a pseudo-$\mathscr{A}_1$ term, the Q band splits significantly in the case of $C_{18}H_{18}$-based perimeters due to the inherent nondegeneracy of the Q excited states of the parent perimeter, even in instances such

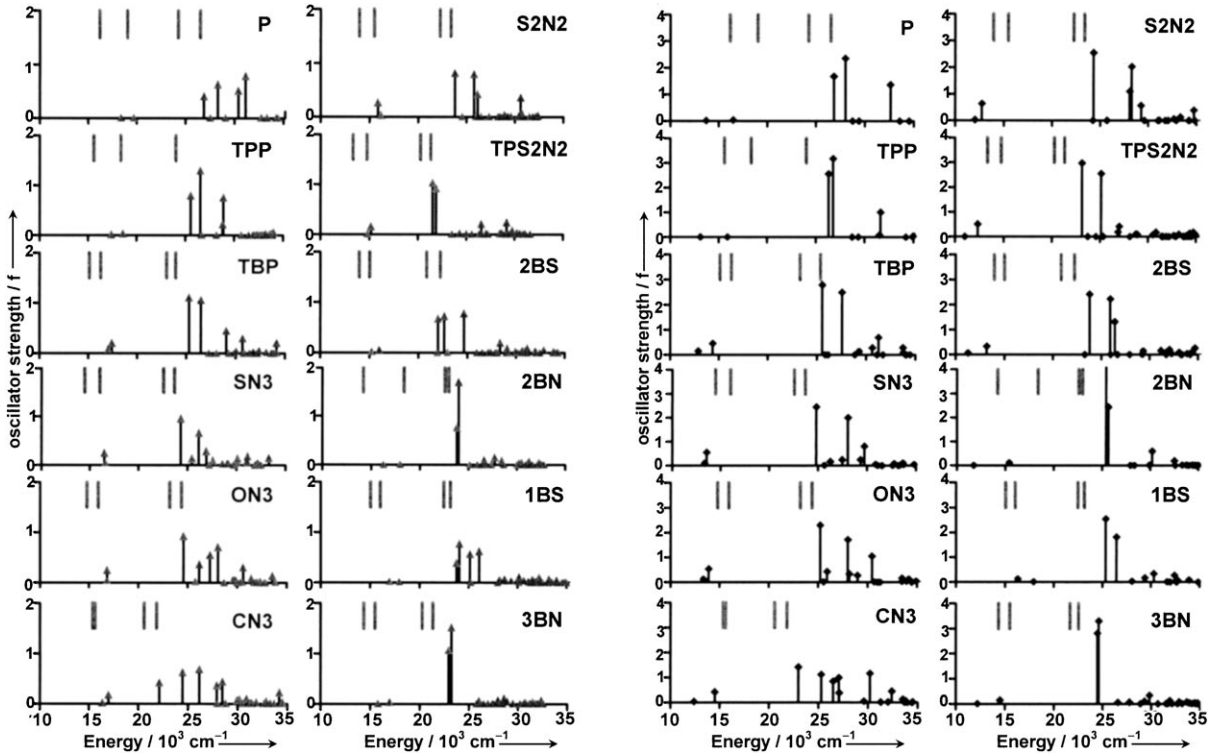

Figure 7. Calculated spectra from TD-DFT (left) and INDO/s (right) calculations from the same set of B3LYP geometry optimizations. Band centers are indicated with triangles and diamonds, respectively. Vertical gray lines indicate the experimentally observed energies of the Q and B bands (Table 1 and Table S2 in the Supporting Information). The spectra of **CSN2**, **OSN2**, **TPTBP** and **TPS2N2** are provided as Figure S6 in the Supporting Information.

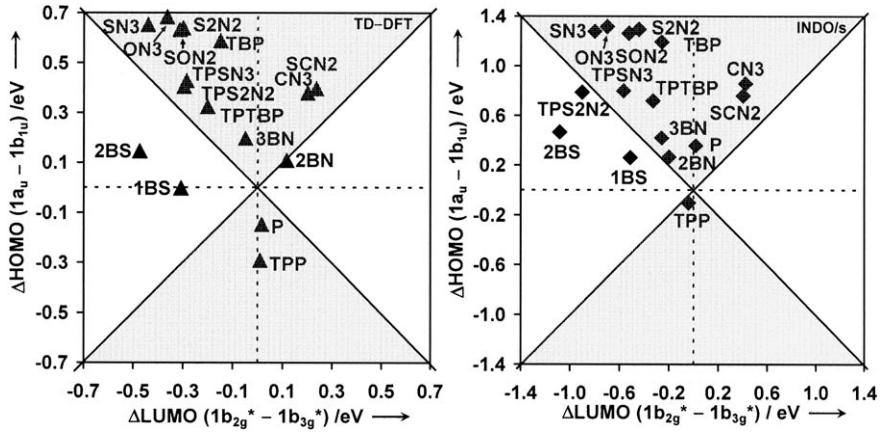

Figure 8. The ΔHOMO and ΔLUMO values predicted by B3LYP (left) and by INDO/s (right) calculations for the same set of B3LYP optimized geometries of **P**, **TPP, TBP**, **SN3**, **ON3**, **CN3**, **S2N2**, **OSN2**, **TPSN3**, **TPS2N2**, **1BS**, **3BN**, **2BN 2BS**, and **CSN2**. In the light gray shaded areas where ΔHOMO > ΔLUMO the normal −, +, −, + MCD sign sequence is anticipated on the basis of Michl's perimeter model[19] for the Q and B bands in ascending energy terms, while a +, −, +, − MCD sign sequence is expected when ΔLUMO > ΔHOMO. Key data are given in Table S3 in the Supporting Information

as **TPP**, the HOMOs and LUMOs of which are accidentally degenerate (Figures 3 and 8). Since ΔHOMO ≈ ΔLUMO ≈ 0 (Figure 8) the spectra of **2BN** can be predicted to mimic that of an ideal $C_{18}H_{18}$ perimeter based on the MO energies predicted for the four frontier π MOs at the B3LYP optimized geometry. This is also reflected in the analysis of dominant ring currents based on the NMR data (Figure 1). The spectrum of **3BN** is also somewhat similar to that of **TPP** for the same reasons (Figure 8).

Both B3LYP and INDO/s calculations successfully predict the trend observed in the intensity of the Q band (Figures 3 and 8, Table 1 and Table S1 in the Supporting Information) and, as was the case in our earlier study on 17 radially symmetric Zn^{II} porphyrinoids.[15] The Q-band intensity of the saddled 5,10,15,20-tetraphenyl TBPs (**TPTBP**, **TPSN3**, and **TPS2N2**) is lower than that of the planar unsubstituted TBPs (**TBP**, **SN3**, and **S2N2**), whereas peripheral substitution of **P** with fused benzene rings to form **TBP** results in increased Q-band intensity. Michl has demonstrated, based on a perimeter-model approach, that the intensity of the Q band is related to the ΔHOMO value, since this determines the degree to which the magnetic properties of the Q and B excited states of the parent perimeter mix [Eqs. (1)–(3)]. The

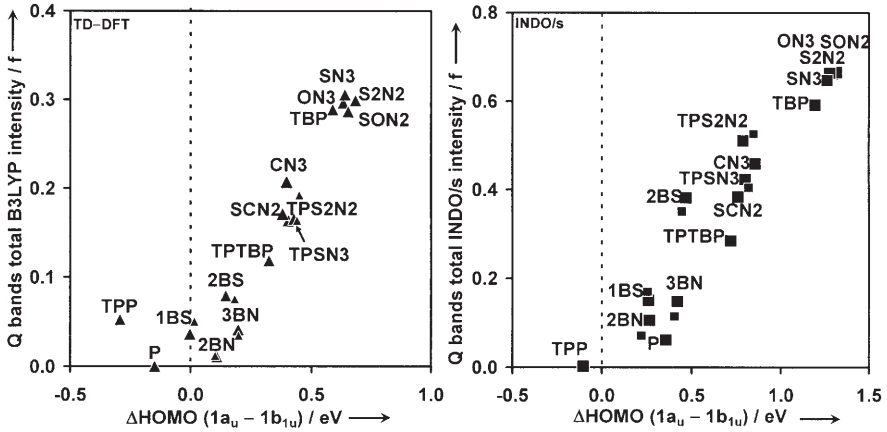

Figure 9. Total Q-band intensity predicted by B3LYP (left) and INDO/s (right) calculations. The smaller plotted values denote the Q-band intensities calculated for the X-ray structures of **TPS2N2**, **TPSN3**, **1BS**, **2BS**, **2BN**, and **3BN**. Key data are given in Table S2 in the Supporting Information.

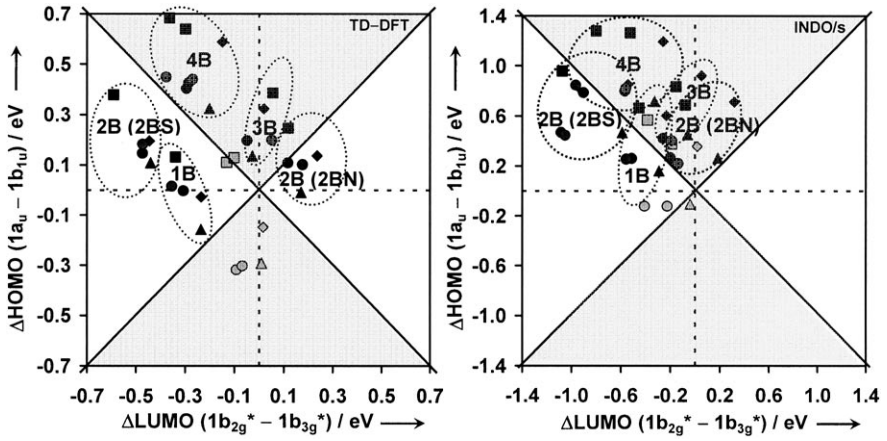

Figure 10. Effect of structural perturbations on the ΔHOMO and ΔLUMO values predicted by B3LYP (left) and by INDO/s (right) calculations for the same set of B3LYP optimized geometries. In the light gray shaded areas where ΔHOMO > ΔLUMO the normal −/+/−/+ MCD sign sequence is anticipated on the basis of Michl's perimeter model[19] for the Q and B bands in ascending energy terms, while a +/−/+/− MCD sign sequence is anticipated when ΔLUMO > ΔHOMO. **P**, monobenzo[*b*]-21*H*,23*H*-porphyrin, opp-dibenzo[*b*,*g*]-21*H*,23*H*-porphyrin, opp-dibenzo[*l*,*q*]-21*H*,23*H*-porphyrin, tribenzo[*b*,*g*,*l*]-21*H*,23*H*-porphyrin, and TBPs are denoted by diamonds. The corresponding 5,10,15,20-tetraphenyl analogues are denoted by triangles, while squares are used for 21-thia-23*H*-porphyrin-21,23-dithiaporphyrin, monobenzo[*b*]-21-thia-23*H*-porphyrin, opp-dibenzo[*b*,*g*]-21*H*,23*H*-porphyrin, opp-dibenzo[*b*,*l*]-21,23-dithiaporphyrin, tribenzo[*g*,*l*,*q*]-21-thia-23*H*-porphyrin, **SN3**, and **S2N2**. The corresponding 5,10,15,20-tetraphenyl analogues, including **1BS**, **2BN**, **2BS**, **3BN**, **TPS2N2** and **TPSN3**, are denoted by circles. The compounds are identified on the basis of number of peripheral fused benzene rings and, in the case of the opp-dibenzoporphyrins, whether the two p_z atomic orbitals on the inner perimeter containing lone pairs are located along the axis with fused benzene rings (**2BS**) or not (**2BN**).

5,10,15,20-tetraphenyl TBPs show significant folding of the heteroaromatic π system due to steric interactions at the ligand periphery, and thus significantly less configuration interaction is predicted between the B excited states and higher energy ππ* states, since the higher energy π MOs are primarily located on the fused benzene rings, whereas the four frontier π MOs are primarily located on the 16-atom inner perimeter. It is noteworthy that TD-DFT calculations appear to markedly overestimate the degree of interaction between the B excited states and higher energy ππ* states (Figures 3 and 7) in the case of non-saddle-shaped compounds.[19] This is most marked in **ON3**, **OSN2**, **CN3**, and **1BS**, for which the strongest interaction between the B and higher energy ππ* states is predicted (Table 1). Even in the case of **P** and **TPP**, two sets of intense, coupled, oppositely signed Faraday $\mathscr{B}_0$ terms are predicted in the UV region. However, this pattern is not observed in the spectrum of TPP (Figure 3), or in the corresponding spectra for ZnTPP and $[H_4TPP]^{2+}$.[15] While a second set of bands can certainly be observed in MCD spectrum of H_2OEP (Figure 3), these bands are usually assigned as being vibrational in origin since a single intense $\mathscr{A}_1$ term is observed for $[H_4OEP]^{2+}$ (Figure 3) and ZnOEP.[15] Although DFT calculations provide significantly better descriptions of the ground state properties of porphyrinoids and TD-DFT calculations more accurately predict the energy gap between the Q and B bands (Figure 13), it is clear from these results that DFT-based calculations do not necessarily always provide an accurate description of the excited-state properties and that MCD spectral data therefore provide a key additional test of their validity.

When MCD spectra[27] were reported previously for 5,10,15,20-tetraphenyltetrabenzo[*b*,*g*,*l*,*q*]porphyrin (**TPTBP**) the normal −, +, −, + sign sequence was reported for the Q and B bands in ascending energy terms. The question of MCD sign sequences was not studied in depth, because the extent and effect of saddling in sterically crowded porphyrinoids was not fully understood at the time. The MCD spectra of most of the core-modified compounds exhibit the same sign sequence as **TBP** and **TPTBP** (Figure 3). An anomalous +, −, −, + sequence is observed for **1BS** and **2BS**, however. When the MCD spectra of the chlorins was studied in detail, Djerassi and coworkers[28] found that when α is relatively small and $|\Delta LUMO - \Delta HOMO| \approx 0$, the MCD sign sequence initially re-

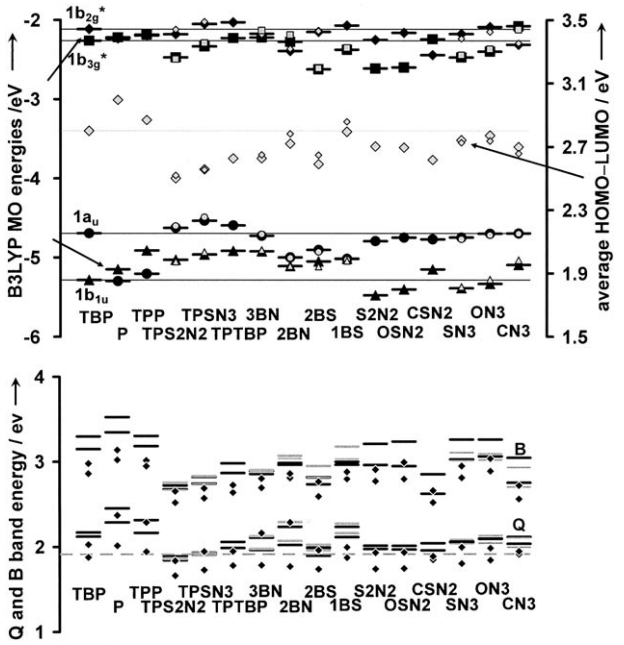

Figure 11. Top: Energies of the four frontier π MOs from Gouterman's four-orbital model[20] predicted by B3LYP and the average HOMO–LUMO band gap based on all four frontier π-MOs. The nodal patterns of the four frontier π MOs of **TBP** are shown at an isosurface value of 0.05 a.u. (Figure 12). Although point-group symmetry changes from compound to compound (Figure 4), these orbitals can still be readily identified based on the characteristic $M_L=\pm4$ and $M_L=\pm5$ nodal patterns (see Figure S3 in the Supporting Information). The smaller set of gray data points are based on TD-DFT calculations on the X-ray structures (Figure 5) in the case of **TPS2N2**, **TPSN3**, **1BS**, **2BS**, **2BN**, and **3BN** and adjacent tautomers in the case of **SN3**, **ON3**, and **CN3**. Bottom: The average energies of the calculated and observed Q and B bands exhibit a trend that is very similar to that observed in the plot of average HOMO–LUMO band gaps against the secondary axis (top). The experimentally observed Q- and B-band energies are shown by black diamonds, and the calculated bands by black horizontal lines in the case of the B3LYP optimized structures (Figure 4), and gray lines for X-ray structures in the case of **TPS2N2**, **TPSN3**, **1BS**, **2BS**, **2BN**, and **3BN** and for B3LYP optimizations of the adjacent tautomers in the case of **SN3**, **ON3** and **CN3**. The dashed horizontal line indicates the upper limit of the region of the spectrum that is useful for PDT. The corresponding INDO/s calculated data are plotted in Figure S7 in the Supporting Information. Key data are given in (Tables S2 and S3 in the Supporting Information).

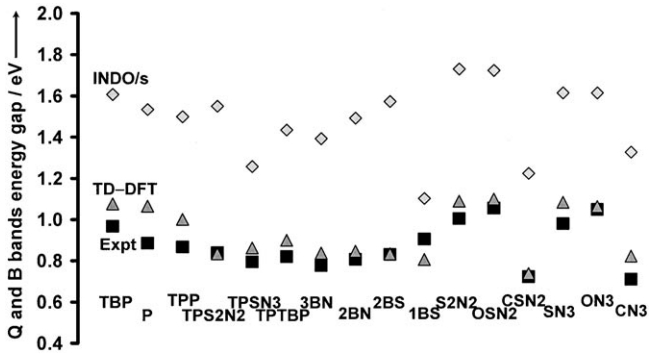

Figure 12. Nodal patterns of the four frontier π MOs of **TBP** at an isosurface value of 0.05 a.u. in both the *xz* and *xy* planes. Numbered dashed lines denote the radial nodal planes of the four frontier π MOs. The $M_L=\pm4$ and $M_L=\pm5$ nodal patterns of the HOMOs and LUMOs of the parent perimeter can be readily identified. The nodal patterns of the other compounds and the parent perimeters are provided at an isosurface value of 0.04 a.u. as Figure S3 in the Supporting Information. Although the point-group symmetry changes from compound to compound (Figures 1 and 4), these MOs can still be readily identified based on the characteristic $M_L=\pm4$ and $M_L=\pm5$ nodal patterns (see Figure S3 in the Supporting Information, as is predicted in Michl's perimeter model (Figure 2).[19]

verses only in the case of the Q band, since the μ^- moment remains the dominant factor for the B band. The values for ΔHOMO and ΔLUMO derived for the B3LYP optimized geometries of **TPP**, **TBP**, **SN3**, **ON3**, **S2N2**, **OSN2**, **CN3**, **CSN2**, **TPSN3**, **TPS2N2**, **1BS**, **3BN**, **2BN**, and **2BS** are shown in Figure 8. The observed sign sequences (Figure 3) in the Q-band region match those that would be predicted on the basis of the ΔHOMO and ΔLUMO values derived from the B3LYP calculations. In the case of INDO/s calculations using the same set of B3LYP-derived geometries, only **TPS2N2** lies outside the observed trend. It is safe to conclude on the basis of the MCD spectra of the nonplanar core-modified benzoporphyrins that nonplanarity usually does not reverse the sequence that would normally anticipated by Michl's perimeter model[19] when ΔHOMO≠ΔLUMO and a significant μ^+ contribution is introduced into the system. The anomalous +, −, +, − sign sequence observed for ZnTPTANP was ascribed, on the basis of TD-DFT and INDO/s calculations, to formation of a "double-soft MCD chromophore" in which ΔHOMO≈ΔLUMO ≈0.[15] The Q band is fully forbidden in electronic terms, which eliminates the μ^+ contribution to the spectrum. The high degree of saddling of the ligand reverses the alignment of the μ^- moment of ZnTPTANP, since the OAM associated with the LUMO is quenched to a greater extent than that associated with the HOMOs due to greater electron density being located on the peripheral fused acenaphthalenes.

There has been considerable controversy in the literature in recent years over whether redshifts of porphyrinoid Q and B bands can be related directly to the extent and nature of ligand nonplanarity. Shelnutt and co-workers[14a,b] proposed, based on molecular mechanics and INDO/s calculations, a direct correlation between the magnitude of the observed redshifts of the Q_{00} and B_{00} bands of sterically hindered porphyrins and the degree and nature of ligand nonplanarity. In contrast, di Magno pointed to substituent effects as the major cause, based on in-plane nuclear reorganization.[14d] Since the energies and intensities of the Q and B excited states in Gouterman's four-orbital model are described in terms of complex rather than real wavefunctions, the INDO/s spectrum for an ideal $C_{16}H_{16}^{2-}$ or $C_{18}H_{18}$ perimeter contain 50% contributions from the two possible HOMO→LUMO transitions (Table 1 and Table S1 in the Supporting Information). Perturbations to the structure result in reduced mixing of the Q and B excited states, so that the Q band becomes electronically allowed (Table 1 and Figure 9). The energies of all four frontier π MOs there-

Table 1. The contribution from Gouterman's four-orbital model[20] transitions to the Q_{00} and B_{00} transitions in the INDO/s calculated spectra of the $C_{18}H_{18}$ parent perimeter, **TBP**, **P**, **TPS2N2**, **TPSN3**, **TPTBP**, **3BN**, **2BN**, **2BS**, **1BS**, **S2N2**, **SN3**, **ON3**, and **CN3** based on B3LYP geometry optimizations.

	Q [%][a]		B [%][a]		4-orb[b]		Int. (f)[c]	
					Q	B	Q	B
$C_{18}H_{18}$	11140	16420	29530	29530	**97**	**98**	0.00	4.72
	(48:48)	(49:49)	(49:49)	(49:49)			0.00	4.72
TBP	12880	14380	25540	27540	**96**	**87**	0.15	2.79
	(64:32)	(80:18)	(29:53)	(17:74)			0.45	2.50
P	13700	16490	26830	28020	**97**	**83**	0.02	1.67
	(52:44)	(59:39)	(35:37)	(37:57)			0.04	2.36
TPP	13110	15890	26310	26780	**97**	**87**	0.00	2.55
	(51:46)	(49:49)	(35:47)	(47:47)			0.00	3.17
TPS2N2	11000	12330	23120	25140	**97**	**91**	0.00	2.96
	(44:52)	(84:14)	(49:39)	(12:80)			0.51	2.54
TPSN3	13390	14760	23250	25120	**96**	**89**	0.40	2.60
	(84:14)	(55:41)	(37:49)	(13:78)			0.03	1.88
3BN	12190	14490	24460	24610	**97**	**91**	0.00	2.81
	(49:46)	(68:30)	(44:45)	(28:64)			0.15	3.29
2BN	11730	15370	25430	25670	**97**	**89**	0.00	4.08
	(49:47)	(64:34)	(32:61)	(43:42)			0.11	2.44
2BS	11240	13170	23790	25920	**97**	**83**	0.06	2.42
	(35:61)	(82:16)	(50:23)	(14:78)			0.33	2.23
1BS	16300	17930	25320	26440	**96**	**91**	0.14	2.54
	(75:22)	(38:57)	(55:33)	(21:73)			0.01	1.81
S2N2	12030	12760	24320	28270	**97**	**83**	0.03	2.55
	(57:39)	(87:11)	(34:45)	(10:78)			0.63	2.04
SN3	13340	13550	24820	28060	**97**	**77**	0.10	2.45
	(63:33)	(85:13)	(28:48)	(11:68)			0.55	2.00
ON3	13340	13880	25220	27990	**97**	**70**	0.13	2.30
	(64:32)	(84:13)	(22:42)	(11:65)			0.54	1.71
CN3	12400	14510	22980	25300	**96**	**58**	0.05	1.42
	(52:43)	(79:19)	(31:38)	(9:37)			0.41	1.12
OSN2	12140	12910	24510	28260	**97**	**69**	0.05	2.19
	(58:38)	(87:11)	(28:38)	(8:65)			0.62	1.40
CSN2	13170	14240	22470	24640	**96**	**71**	0.07	1.21
	(56:39)	(77:20)	(28:43)	(20:52)			0.31	1.89

[a] Energies of the Q_{00} and B_{00} bands in ascending order. The percentage contributions of the $1a_u \rightarrow 1_{b2/3g}$ and $1b_{1u} \rightarrow 1b_{2/3g}$ one-electron transitions (Figure 2) are given in parentheses in the lower row. [b] Combined contribution from the four one-electron transitions in Gouterman's four-orbital model to the Q and B bands. The contribution to the B band is often significantly less than 100% due to configuration interaction with higher energy $\pi\pi^*$ states. [c] Predicted oscillator strengths of the Q and B bands. The values for the lower energy Q and B bands are listed above those for the higher energy bands. Key data for X-ray structures of **TPS2N2**, **TPSN3**, **3BN**, **2BN**, **2BS** and **1BS** are provided in Table S1 in the Supporting Information.

fore must be taken into account. When this factor is taken into consideration, correlation between the observed averaged energies of the symmetry-split Q and B bands and the averaged band gap (LUMO – HOMO) energies predicted by both B3LYP and INDO/s calculations is strong (Figure 11). There is a marked redshift of the B band due to reduced configuration interaction between the B excited state and higher energy $\pi\pi^*$ states (Table 1 and Table S1 in the Supporting Information. Therefore, when the four-orbital model is the dominant factor in determining the energies of the optically accessible excited states in the UV/Vis region, structural perturbations at the ligand periphery result in systematic redshifts similar to those reported by Shelnutt and co-workers.[14a,b] The fact that the band centers predicted in the TD-DFT calculations for the six X-ray structures differ somewhat from those in the B3LYP optimized structures also points to core modes of vibration such as saddling and ruffling being a key factor, as Shelnutt and co-workers reported. However, the spectral data derived from core-modified tetrabenzoporphyins (Figures 3 and 4) demonstrate that a redshift is not always diagnostic of porphyrinoid nonplanarity. The Q and B bands of **SN3**, **S2N2**, and **OSN2** and the Q bands of **ON3** are red-shifted relative to those of **TBP** due to stabilization of the $1b_{3g}$* LUMO, since a major node is located on the more electronegative sulfur or oxygen atom.

Conclusion

Even in the case of core-modified and nonplanar sterically crowded porphyrinoids, the OAM properties of the four frontier π-MOs largely determine the optical properties. Despite the large structural perturbations introduced by core modification of the pyrrole nitrogen atoms, only minor effects are observed in the optical spectra of **SN3**, **S2N2**, **ON3**, and **OSN2** based on slight shifts in the band-center wavelengths and changes in band intensity, since the lone pair of N–H is directly replaced by that of a sulfur or an oxygen atom. Greater effects are observed on core modification with carbon atoms, since the carbon $2p_z$ atomic orbital is singly occupied and a lone pair is effectively transferred to a pyrrole nitrogen atom on the other in-plane axis of the π system in the case of **CN3** and **CSN2**. Even in the absence of DFT-based calculations of MCD spectra, analysis of MCD spectral data with Michl's perimeter model[19] can provide a key additional test of the validity of TD-DFT descriptions of the geometries and optical properties of porphyrinoids based on the orbital angular momentum properties of the heteroaromatic π system. Although analysis of certain aspects of the TD-DFT results remains problematic, theoretical calculations have clearly advanced to the point that target porphyrinoids can be designed that are likely to exhibit a desired set of electronic and/or optical properties based on trends observed in the spectra for a wide range of different porphyrinoids.

Experimental Section

Optical spectroscopy: Electronic absorption spectra were measured with a Jasco V-570 or a Cary 5G spectrophotometer. Magnetic circular dichroism (MCD) spectra[17] were recorded with a Jasco J-725 spectrodichrometer and a Jasco electromagnet that produces a magnetic field of up to 1.09 T, or with a Jasco J-810 spectrodichrometer and an Oxford Instruments SM2 cryomagnet with a maximum field strength of 5.0 T. The field strength and sign were calibrated by measuring the MCD spectrum of an aqueous solution of $CoSO_4$ at 510 nm ($\Delta\varepsilon_M = -1.8969\ L\,mol^{-1}\,cm^{-1}\,T^{-1}$). The signal intensity of the CD spectrometer was also tested with ammonium *d*-camphor-10-sulfonate to ensure that the θ/A ratio for the peaks at 280 nm was 2.26.[29] Spectral-grade dimethylformamide (DMF) was

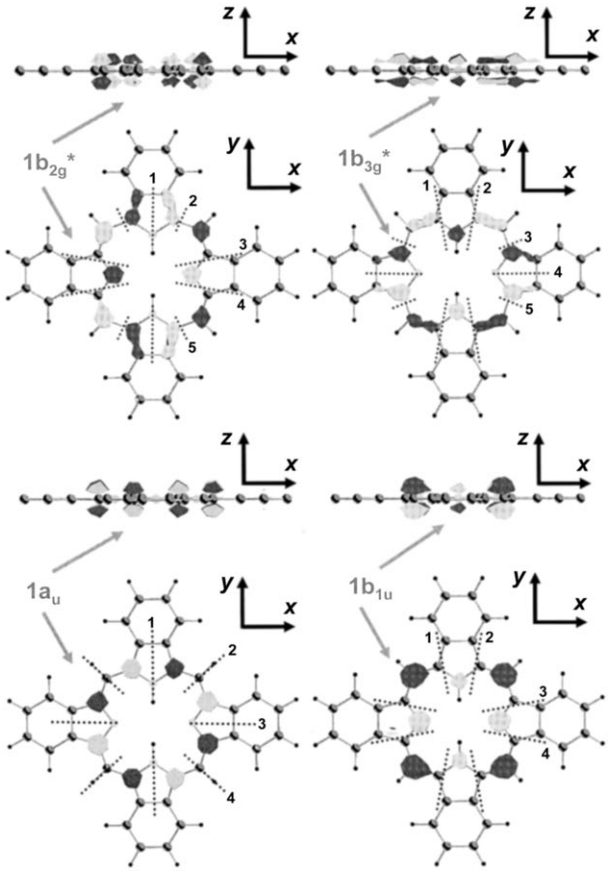

Figure 13. Average energy gap between the Q and B bands. The experimentally observed values are denoted by black squares, while the TD-DFT and INDO/s calculated values are denoted with dark gray triangles and light gray diamonds, respectively. Key data are provided as (see Table S2 in the Supporting Information).

purchased from Aldrich along with H_2OEP and H_2TPP. $[H_4OEP]^{2+}$ was prepared by adding a trace of trifluoroacetic acid (TFA).

Synthesis

General: Melting points were measured with a Yanaco M500-D melting point apparatus. IR spectra were measured on a Hitachi 270-30 as KBr disks. FAB and DI-EI mass spectra were measured on a JEOL JMS-700 spectrometer. MALDI-TOF mass spectra were measured on a Voyager DE Pro instrument (Applied Biosystems). Elemental analyses were performed on a Yanaco MT-5 elemental analyzer. All solvents and chemicals were of reagent-grade quality, obtained commercially, and used without further purification except as noted. Dry dichloromethane and THF were purchased from Kanto Chemical Co. Toluene, hexane, triethylamine, pyridine, 1,8-diazabicyclo[5.4.0]undec-7-ene (DBU), and chloroform were distilled from calcium hydride and then stored on appropriate molecular sieves. Solvents for chromatography were purified by distillation. Thin-layer (TLC) and column chromatography were performed on Art. 5554 (Merck KGaA) and Silica Gel 60N (Kanto Chemical Co.), respectively. For spectral measurements, spectral-grade toluene and chloroform was purchased from Nacalai Tesque Co.

ON3 and CSN2: A [3+1] approach using a bicyclo[2.2.2]octadiene-fused (BCOD-fused) tripyrrane analogue, similar to that reported previously for **SN3**, **S2N2**, **OSN2** and **CN3**, was employed.[11a] In order to apply common porphyrin synthetic pathways such as the Lindsey [2+2] and [3+1] methods,[30] a BCOD-fused furan with formyl and hydroxymethyl groups at the α positions and BCOD-fused tripyrranes was required for **ON3**, and BCOD-fused diformylindene for **CSN2**.

BCOD-fused diformylindene: The synthesis of diformylindene (**10**) has been reported previously.[30]

BCOD-fused furan dicarbaldehyde: Diformylation of the previously reported BCOD-fused furan **2**[32] was required (Scheme 1). Compound **2** was prepared by using a slightly modified procedure reported previously by Gorgues et al..[32] Formylation under the direct diformylation conditions, used previously for the preparation of diformylpyrrole,[10b] gave an intractable resinous material. Since this was probably due to the labile nature of **2** under acidic conditions, formylation was attempted under basic conditions. Treatment of **2** with *n*BuLi in THF at −78 °C followed by quenching with DMF afforded monoformylated furan **6** in 81 % yield,[9] and diformylation was unsuccessful. We therefore adopted an indirect synthetic route. Protection of furancarbaldehyde **6** with ethylene acetal gave **7** in 93 % yield. Lithiation of **7** with *n*BuLi followed by quenching with DMF afforded the monoacetal of the furandicarbaldehyde, which was hydrolyzed under mild acidic conditions to give the targeted furandicarbaldehyde **3** in 67 % yield from **7**.

4,7-Dihydro-4,7-ethanoisobenzofuran-1-carbaldehyde (6): A 1.58 M solution of *n*BuLi (9.87 mL, 15.6 mmol) in hexane was added to a stirred solution of **2** (2.08 g, 14.2 mmol) in dry THF (60 mL) at −78 °C and the mixture was then stirred at −10 °C for 30 min. After the mixture was cooled to −78 °C, dry DMF (5 mL) was added slowly with stirring. The mixture was allowed to warm to room temperature and stirring was continued for 6 h. The mixture was then poured into a saturated aqueous ammonium chloride solution (50 mL) and extracted with diethyl ether. The ethereal layer was washed sequentially with water and brine, dried over Na_2SO_4, and concentrated. Chromatography on silica gel (20 % EtOAc/hexane) followed by recrystallization from $CHCl_3$/hexane yielded **6** (2.00 g, 11.5 mmol; 81 %) as pale yellow crystals: R_f = 0.26 (10 % EtOAc/hexane); m.p. 56–57 °C; ^{1}H NMR ($CDCl_3$): δ = 9.66 (s, 1H), 7.24 (s, 1H), 6.55–6.44 (m, 2H), 4.32 (m, 1H), 3.92 (m, 1H), 1.72–1.50 ppm (m, 4H); ^{13}C NMR ($CDCl_3$): δ = 177.0, 142.8, 136.2, 136.1, 135.5, 133.8, 133.7, 31.9, 31.2, 25.9, 25.5 ppm; MS (EI): *m*/*z* (%): 174 (12) $[M]^+$, 146 (100); IR (KBr): $\tilde{\nu}$ = 3112, 2942, 2869, 1658, 1531, 1407, 1380, 1311, 1288 cm^{-1}; elemental analysis calcd (%) for $C_{11}H_{10}O_2$: C 75.84, H 5.79; found: C 76.02, H 5.82.

1-([1,3]Dioxolan-2-yl)-4,7-dihydro-4,7-ethanoisobenzofuran (7): A benzene solution (80 mL) of **6** (2.53 g, 14.5 mmol), pyridinium tosylate (0.10 g), and ethylene glycol (2.69 g, 43.5 mmol) was placed in a 200 mL round-bottomed flask equipped with a Dean–Stark apparatus and was refluxed for 2 h under nitrogen. After the mixture was cooled to room temperature, diethyl ether was added. The mixture was washed with saturated aqueous $NaHCO_3$, water, and brine, dried over Na_2SO_4, and concentrated. The residue was purified by chromatography on silica gel (20 % EtOAc/hexane) to give **7** (2.95 g, 13.5 mmol; 93 %), which was solidified in a freezer: R_f = 0.48 (20 % EtOAc/hexane); m.p. 37–39 °C; ^{1}H NMR ($CDCl_3$): δ = 7.01 (s, 1H), 6.46–6.41 (m, 2H), 5.94 (s, 1H), 4.15–4.08 (m, 2H), 4.04–3.97 (m, 2H), 3.90 (m, 1H), 3.79 (m, 1H), 1.58–1.52 ppm (m, 4H); ^{13}C NMR ($CDCl_3$): δ = 138.4, 135.1, 134.8, 131.3, 131.0, 130.2, 97.4, 65.1, 65.0, 31.3, 31.2, 26.4, 26.3 ppm; MS (EI): *m*/*z* (%): 218 (32) $[M]^+$, 190 (100), 162 (47); IR (KBr): $\tilde{\nu}$ = 3058, 2958, 2869, 1673, 1403, 1268, 1133, 1099, 1022, 944 cm^{-1}; elemental analysis calcd (%) for $C_{13}H_{14}O_3$: C 71.54, H 6.47; found: C 71.56, H 6.52.

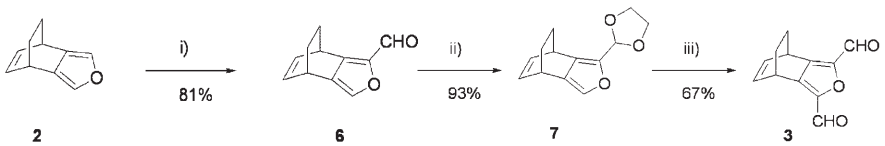

Scheme 1. Preparation of 4,7-ethanoisobenzofuran. Reagents and conditions: i) *n*BuLi, THF, −78 °C, 30 min; DMF, RT, 14 h; ii) ethylene glycol, pyridinium tosylate, reflux, 2 h; iii) *n*BuLi, THF, −78 °C, 30 min; DMF, RT, 14 h; pyridinium tosylate, water/acetone, reflux, 14 h.

4,7-Dihydro-4,7-ethanoisobenzofuran-1,3-dicarbaldehyde (3): A 1.43 M solution of *t*BuLi (3.50 mL, 5.00 mmol) in hexane was added to a stirred solution of **7** (0.655 g, 3.00 mmol) in dry THF (15 mL) at −78 °C under nitrogen. The mixture was then stirred for 30 min. Dry DMF (1 mL) was added slowly with stirring at the same temperature. After addition, the mixture was allowed to warm to room temperature and stirring was continued for 6 h. The mixture was then poured into a saturated aqueous ammonium chloride solution (10 mL) and was extracted with diethyl ether. The ethereal layer was washed with water and brine, dried over Na_2SO_4, and concentrated to leave an oily residue, which was dissolved in water/acetone (20/20 mL). Pyridinium tosylate (0.056 g) was added and the solution was then refluxed overnight. The mixture was cooled to room temperature and saturated aqueous $NaHCO_3$ solution (10 mL) was added. The mixture was extracted with CH_2Cl_2. The organic layer was washed sequentially with water, saturated aqueous $NaHCO_3$, water, and brine, dried over Na_2SO_4, and concentrated. Chromatography on silica gel (30% EtOAc/hexane) followed by recrystallization from $CHCl_3$/hexane yielded **3** (0.411 g, 2.03 mmol; 67%) of as yellow crystals: R_f = 0.48 (20% EtOAc/hexane); m.p. 150–152 °C; ^{1}H NMR ($CDCl_3$): δ = 9.84 (s, 2H), 6.53 (m, 2H), 4.42 (m, 2H), 1.69 (m, 2H), 1.58 ppm (m, 2H); ^{13}C NMR ($CDCl_3$): δ = 179.4, 142.9, 142.0, 134.3, 31.9, 25.3 ppm; MS (EI): *m*/*z* (%): 202 (10) $[M]^+$, 174 (100), 145 (25), 115 (22), 89 (75); IR (KBr): $\tilde{\nu}$ = 2942, 2869, 1681, 1666, 1253, 1141, 1002, 883, 852 cm^{-1}; elemental analysis calcd (%) for $C_{12}H_{10}O_3$: C 71.28, H 4.98; found: C 69.74, H 5.03.

BCOD-fused furan tripyrranes: The tripyrranes required for [3+1] condensation reactions were synthesized according to procedures reported previously.[11a]

Synthesis of BCOD-fused ON3 and CSN2: The method used to synthesize BCOD-fused **ON3** and **CSN2** is shown in Scheme 2. **8a** or **8b** (1.00 mmol) and a magnetic stirring bar were placed in a 500-mL round-bottomed flask, which was thoroughly wrapped with aluminum foil and then flushed with nitrogen. TFA (2.5 mL, 34 mmol) was added and the mixture was stirred for 5 min under nitrogen and then diluted with dry CH_2Cl_2 (200 mL). A dicarbaldehyde (1.00 mmol) was then added. After the mixture was stirred at room temperature overnight, triethylamine (4.8 mL, 34 mmol) was slowly added to neutralize the mixture. 2,3-Dichloro-5,6-dicyanobenzoquinone (DDQ) (0.272 g, 1.20 mmol) was added and the mixture was then stirred for 2 h at room temperature, washed successively with water, saturated aqueous $NaHCO_3$, water, and brine, dried over Na_2SO_4, and concentrated. The[3+1] condensation of **8a** with diformylindene **10**[31] gave TBCOD-fused carbabenzoporphyrin **TBCODCSN2**[11b] in 6% yield. When the previously reported tripyrrane **8b**[11a] was treated with furandicarbaldehyde **3** under acidic conditions, TBCOD-fused oxaporphyrin **TBCODON3** was obtained in 10% yield. The residue was purified by chromatography on basic alumina with an appropriate solvent mixture. Recrystallization yielded **TBCODON3** or **TBCODCSN2** as a mixture of diastereomers.

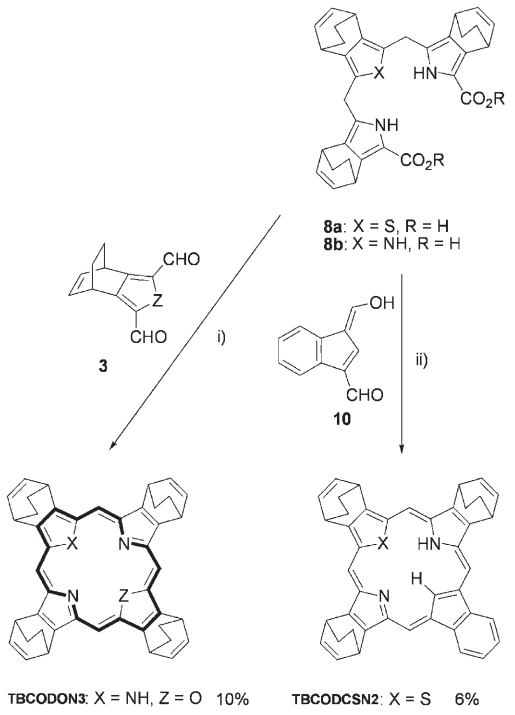

Scheme 2. Preparation of *meso*-unsubstituted core-modified BCOD-fused **ON3** and **CSN2**. Reagents and conditions: i) **3**, TFA, CH_2Cl_2, RT, 16 h; Et_3N, DDQ; ii) **10**, TFA, CH_2Cl_2, RT, 16 h; Et_3N, DDQ.

General procedure for the preparative retro-Diels–Alder reaction: Expansion of the π system by thermal transformation of the fused BCOD groups into benzo moieties was carried out under the conditions reported previously (230–250 °C, 30 min, ca. 0.2 mmHg).[11a] The products obtained are shown in Figure 1 with their carbon numbering schemes.[33] The precursor BCOD-fused porphyrin was placed in a sample tube in a 25 mL round-bottomed flask. The flask was then evacuated with a rotary vacuum pump and heated at 230 °C for 30 min (*meso*-unsubstituted precursors) or for 1 h (*meso*-tetraaryl precursors) in a glass tube oven. After cooling, the target core-modified benzoporphyrin was obtained in quantitative yield.

22*H*,21,23-Thiacarbatetrabenzo[*b*,*g*,*l*,*q*]porphyrin (CSN2): dark green solid; m.p. >300 °C; UV/Vis (DMF): λ_{max} (lg ε) = 412 (4.48), 440 (4.55), 466 (5.27), 498 (4.97), 623 (4.23), 663 (4.69), 679 nm (4.80); elemental analysis calcd (%) for $C_{37}H_{22}N_2S$: C 84.38, H 4.21, N 5.32; found: C 83.82, H 4.31, N 5.14.

23*H*,21-Oxatetrabenzo[*b*,*g*,*l*,*q*]porphyrin (ON3): black solid; m.p. >300 °C; UV/Vis (DMF): λ_{max} (lg ε) = 383 (4.46), 411 (4.80), 431 (4.92), 608 (4.52), 618 (4.47), 629 (4.36), 678 nm (4.19); elemental analysis calcd (%) for $C_{36}H_{21}N_3O \cdot 0.25\,H_2O$: C 83.78, H, 4.20, N 8.14; found: C 83.50, H 4.34, N 8.05.

TPS2N2, TPSN3, 1BS, 2BS, 2BN and 3BN: The [2+2] and[3+1] Lindsay methods were applied for the preparation of *meso*-tetraaryl-substituted derivatives. BCOD-fused thiophene **5b** with formyl and hydroxymethyl groups at the α positions was required to synthesize all six compounds, BCOD-fused pyrrole **2a** was required to synthesize **TPS2N2**, **TPSN3**, **2BN**, **3BN**, and bis(phenylhydroxymethyl)thiophene (**5b**) was required to synthesize **2BN** and **3BN**.

BCOD-fused pyrrole: 4,7-Dihydro-4,7-ethano-2*H*-isoindole (**2a**) was prepared according to the literature procedure.[10b]

Bis(phenylhydroxymethyl)thiophene: The previously reported[32] diastereomeric bis(phenylhydroxymethyl)thiophene was prepared according to the literature procedure.[12,34]

BCOD-fused thiophene dicarbaldehyde: Since direct formylation by the *ortho*-formate method yielded only the monoformyl derivative, lithiation of **2b** was examined under several different conditions. Treatment of **2b** with 2.5 equivalents of lithium diisopropylamide (LDA) or *n*BuLi in THF at −10 °C followed by quenching with DMF was also found to result only in the formation of monoformylated compounds. More severe conditions are clearly needed for dilithiation. A diastereomeric mixture of bis(phenylhydroxymethyl)thiophene **5a** was formed in 42% yield by treating thiophene **2b** with 2.5 equivalents of *n*BuLi in *n*-hexane in the presence of benzaldehyde in a similar manner.

1,3-Bis(phenylhydroxymethyl)-4,7-dihydro-4,7-ethano-2-benzothiophene (5a): The introduction of formyl and phenylhydroxymethyl groups into 4,7-dihydro-4,7-ethanoisothianaphthene (**2b**),[9] is illustrated in Scheme 3. A 1.58 M solution of *n*BuLi (22.7 mL, 36.0 mmol) in hexane was added to a stirred solution of **2b** (2.43 g, 15.0 mmol) and *N*,*N*,*N*′,*N*′-tetramethylethylenediamine (TMEDA, 3.56 mL, 36.0 mmol) in dry hexane (50 mL) at room temperature and the mixture was refluxed for 30 min. After the mixture was cooled at −50 °C, dry THF (50 mL) and then benzaldehyde (5.10 mL, 50.0 mmol) were slowly added with stirring. The mixture was allowed to warm to room temperature and stirring was continued overnight. The mixture was poured into a saturated aqueous ammonium chlo-

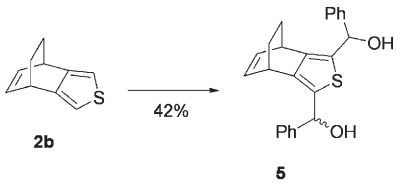

Scheme 3. Preparation of 4,7-ethanoisothianaphthene. Reagents and conditions: *n*BuLi, TMEDA, hexane, reflux, 30 min; PhCHO, THF, −50 °C→RT.

ride solution (50 mL) and was extracted with diethyl ether. The ethereal layer was washed sequentially with water and brine, dried over Na_2SO_4, and concentrated to leave an oily material, which solidified on standing in a refrigerator with a small amount of benzene. Filtration gave **5a** (2.36 g, 6.32 mmol; 42%) as a mixture of diastereomers: m.p. 128–134 °C; ^{1}H NMR ($CDCl_3$): $\delta = 7.44$–7.38 (m, 4H), 7.37–7.30 (m, 4H), 7.30–7.24 (m, 2H), 6.43–6.37 (m, 2H), 6.06–6.01 (m, 2H), 2.20 (br s, 2H), 1.52–1.32 ppm (m, 4H); ^{13}C NMR ($CDCl_3$, typical signals): $\delta = 143.9$, 143.5, 143.3 (2C), 143.2, 143.1, 143.0, 135.2 (3C), 135.1, 133.7, 133.3 (2C), 133.1, 128.4 (2C), 128.3, 127.7 (2C), 127.6, 126.1, 126.0 (3C), 70.7, 70.6, 70.5, 70.4, 35.1, 35.0 (2C), 25.8, 25.7 (2C), 25.6 ppm; MS (EI): *m*/*z* (%): 374 (18) $[M]^+$, 346 (92), 223 (100); IR (KBr): $\tilde{\nu} = 3336$, 3054, 2954, 2865, 1600, 1450, 1033, 1014 cm^{-1}; elemental analysis calcd (%) for $C_{24}H_{22}O_2S$: C 76.97, H 5.92; found: C 76.72, H 6.11.

Synthesis of BCOD-fused TPS2N2, TPSN3, 1BS, 2BS, 2BN, and 3BN: Bis(phenylhydroxymethyl) derivative **5a** was treated with three equivalents of the α-unsubstituted BCOD-fused pyrrole **2a** and two equivalents of *p*-tolualdehyde in the presence of $BF_3{\cdot}OEt_2$ at room temperature, followed by oxidation with chloranil. The tetra-BCOD-fused thiaporphyrin **TBCODTPSN3** with tetraaryl substituents at the *meso*-carbon atoms was obtained in 51% yield. Analogous treatment of **5a** with pyrrole and *p*-tolualdehyde gave mono-BCOD-fused thiaporphyrin **1BCODS** in 23% yield. The[2+2] synthesis of **5a** was expected to provide the opp-dithiaporphyrin. Tetra-BCOD- and bi-BCOD-fused 21, 23-dithiaporphyrins **TBCODTPS2N2** and **2BCODS** were obtained from the reaction of **5a** with one equivalent of **2a** and pyrrole in the presence of $BF_3{\cdot}OEt_2$ at room temperature followed by oxidation with chloranil in 26 and 13% yield, respectively. Using the previously reported bis(phenylhydroxymethyl)thiophene **5b**,[12,34] tri-BCOD-fused thiaporphyrin **3BCODN** and bi-BCOD-fused 22,24-dithiaporphyrin **2BCODN** were obtained in 22 and 12% yield, respectively, in a similar manner (Scheme 4).

General procedure for [2+2] condensation of bis(hydroxymethyl)thiophene 5 and pyrrole: Bis(hydroxymethyl)thiophene **5** (2.00 mmol), pyrrole (2 mmol), and a magnetic stirring bar were placed in a 1 L round-bottomed flask equipped with a reflux condenser, which was thoroughly wrapped with aluminum foil and then flushed with nitrogen. Dry and degassed CH_2Cl_2 (600 mL) and $BF_3{\cdot}OEt_2$ (50 μL, 0.41 mmol) were added successively, and the mixture was then stirred for 1 h at room temperature. Chloranil (0.737 g, 3.00 mmol) was added and the mixture was refluxed for 1 h. The mixture was then concentrated and the residue was purified by chromatography on basic alumina with an appropriate solvent mixture. Recrystallization gave pure core-modified porphyrin as a mixture of diastereomers. The reactions are summarized in Scheme 4.

5,10,15,20-Tetraphenyl-2^1,2^4,7^1,7^4,12^1,12^4,17^1,17^4-octahydro-2^1,2^4;7^1,7^4;12^1,12^4;17^1,17^4-tetraethano-21,23-dithiatetrabenzo-[*b*,*g*,*l*,*q*]porphyrin (TBCODTPS2N2): The reaction of **5a** with **2a** was performed according to the general procedure. The target porphyrin was isolated by chromatography with 3% EtOAc/CH_2Cl_2 as eluent and recrystallization from $CHCl_3$/MeOH in 26% yield as reddish purple crystals: m.p. >130 °C (decomp); ^{1}H NMR ($CDCl_3$): $\delta = 8.38$–8.21 (m, 8H), 7.89–7.80 (m, 12H), 6.74–6.10 (m, 8H), 3.95–3.84 (m, 4H), 3.37–3.27 (m, 4H), 1.98–0.61 ppm (m, 16H); MS (FAB): *m*/*z* (%): 961 (100) $[M+H]^+$, 933 (6), 905 (4), 877 (11), 849 (33); UV/Vis (CH_2Cl_2): λ_{max} ($\lg\varepsilon$) = 443 (5.00), 524 (4.20), 637 (3.46), 714 nm (3.43); elemental analysis calcd (%) for $C_{68}H_{52}N_2S_2{\cdot}2\,CHCl_3$: C 70.06, H 4.54, N 2.33; found: C 69.99, H 4.70, N 2.29.

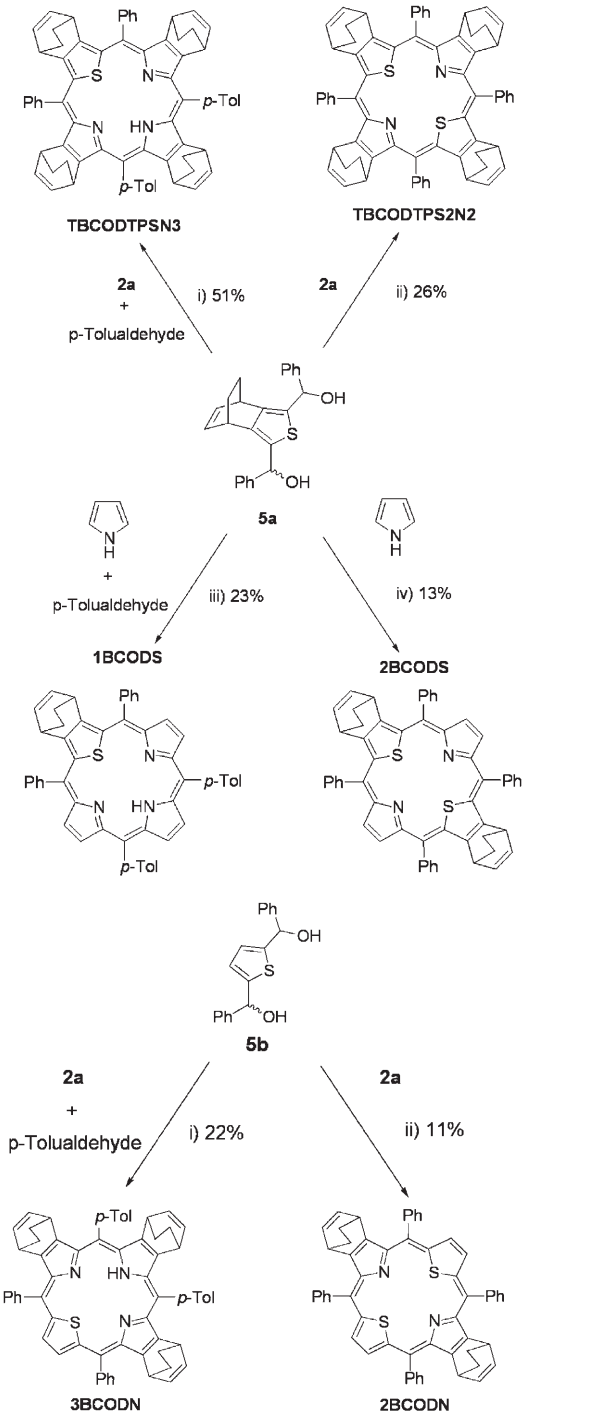

Scheme 4. Top: Preparation of *meso*-tetraaryl core-modified BCOD-fused porphyrins from **5a**. Reagents and conditions: i) **2a** (3.0 equiv), *p*-tolualdehyde (2.0 equiv), $BF_3{\cdot}OEt_2$, $CHCl_3$, RT, 1 h; chloranil, reflux, 1 h; ii) **2a** (1.0 equiv), $BF_3{\cdot}OEt_2$, $CHCl_3$, RT, 1 h; chloranil, reflux, 1 h; iii) pyrrole (3.0 equiv), *p*-tolualdehyde (2.0 equiv), $BF_3{\cdot}OEt_2$, $CHCl_3$, RT, 1 h; chloranil, reflux, 1 h; iv) pyrrole (1.0 equiv), $BF_3{\cdot}OEt_2$, $CHCl_3$, RT, 1 h; chloranil, reflux, 1 h. Bottom: Preparation of *meso*-tetraaryl core-modified BCOD-fused porphyrins from **5b**. Reagents and conditions: i) **2a** (3.0 equiv), *p*-tolualdehyde (2.0 equiv), $BF_3{\cdot}OEt_2$, $CHCl_3$, RT, 1 h; chloranil, reflux, 1 h; ii) **2a** (1.0 equiv), $BF_3{\cdot}OEt_2$, $CHCl_3$, RT, 1 h; chloranil, reflux, 1 h.

5,10,15,20-Tetraphenyl-2^1,2^4,12^1,12^4-tetrahydro-2^1,2^4;12^1,12^4-diethano-21,23 -dithiadibenzo[*b*,*l*]porphyrin (2BCODS): The reaction of **5a** with pyrrole was performed according to the general procedure. The target porphyrin was isolated by chromatography with CH_2Cl_2 as eluent and recrystallization from $CHCl_3$/MeOH in 13% yield as purple crystals: m.p. >130°C (decomp); ^{1}H NMR ($CDCl_3$): δ=8.51 (s, 4H), 8.34–8.16 (m, 8H), 7.87–7.77 (m, 12H), 6.70–6.52 (m, 4H), 4.00 (m, 4H), 1.44–1.06 ppm (m, 8H); MS (FAB): *m*/*z* (%): 805 (100) $[M+H]^+$, 777 (12), 749 (51); UV/Vis (CH_2Cl_2): λ_{max} (lgε)=443 (5.31), 522 (4.32), 639 (3.55), 703 nm (3.80); elemental analysis calcd (%) for $C_{56}H_{40}N_2S_2\cdot0.25\,CHCl_3$: C 80.92, H 4.86, N 3.36; found: C 81.00, H 5.02, N 3.29.

5,10,15,20-Tetraphenyl-2^1,2^4,12^1,12^4-tetrahydro-2^1,2^4;12^1,12^4-diethano-22,24-dithiadibenzo[*b*,*l*]porphyrin (2BCODN): The reaction of **5b** with **2a** was performed according to the general procedure. The target porphyrin was isolated by chromatography with CH_2Cl_2 as eluent and recrystallization from $CHCl_3$/MeOH in 11% yield as brown crystals: m.p. >130°C (decomp); ^{1}H NMR ($CDCl_3$): δ=9.48 (s, 4H), 8.24–8.13 (m, 8H), 7.86–7.76 (m, 12H), 6.47–6.39 (m, 4H), 3.51 (m, 4H) 1.64–1.47 ppm (m, 8H); MS (FAB): *m*/*z* (%): 805 (100) $[M+H]^+$, 777 (15), 749 (66); UV/Vis (CH_2Cl_2): λ_{max} (lgε)=421 (5.27), 511 (4.46), 626 (3.36), 688 nm (3.22); elemental analysis calcd (%) for $C_{56}H_{40}N_2S_2.H_2O$: C 81.72, H 5.14, N 3.40; found: C 81.97, H 5.10, N 3.38.

General procedure for[3+1] condensation of bis(hydroxymethyl)thiophene 5, pyrrole, and *p*-tolualdehyde: Bis(hydroxymethyl)thiophene **5** (1.00 mmol), pyrrole (3.00 mmol), *p*-tolualdehyde (2.00 mmol), and a magnetic stirring bar were placed in a 1 L round-bottomed flask equipped with a reflux condenser, which was thoroughly wrapped with aluminum foil and then flushed with nitrogen. Dry and degassed $CHCl_3$ (600 mL) and $BF_3\cdot OEt_2$ (50 μL, 0.41 mmol) were added successively, and the mixture was then stirred for 1 h at room temperature. Chloranil (0.737 g, 3.00 mmol) was added and the mixture was refluxed for 1 h. The mixture was then concentrated and the residue was purified by chromatography on basic alumina using an appropriate solvent system. Recrystallization yielded pure core-modified porphyrin as a mixture of diastereomers. The reactions are summarized in Scheme 4.

5,20-Diphenyl-10,15-*p*-tolyl-2^1,2^4,7^1,7^4,12^1,12^4,17^1,17^4-octahydro-2^1,2^4;7^1,7^4;12^1,12^4;17^1,17^4-tetraethano-23*H*,21-thiatetrabenzo[*b*,*g*,*l*,*q*]porphyrin (TBCODTPSN3): The reaction of **5a** with **2a** and *p*-tolualdehyde was performed according to the general procedure. The target porphyrin was isolated by chromatography with 2% THF/CH_2Cl_2 as eluent and recrystallization from $CHCl_3$/MeOH in 51% yield as dark brown crystals: m.p. >130°C (decomp); ^{1}H NMR ($CDCl_3$): δ=8.38–8.06 (m, 8H), 7.87–7.80 (m, 6H), 7.67–7.60 (m, 4H), 6.78–6.09 (m, 8H), 4.04 (m, 2H), 3.45 (m, 2H), 3.31 (m, 2H), 3.23 (m, 2H), 2.78 (s, 6H), 1.96–0.59 (m, 16H), −3.35 ppm (brs, 1H); MS (FAB): *m*/*z* (%): 972 (100) $[M+H]^+$, 944 (5), 916 (3), 888 (11), 860 (36); UV/Vis (CH_2Cl_2): λ_{max} (lgε)=437 (5.15), 524 (4.26), 622 (3.65), 685 (3.53); elemental analysis calcd (%) for $C_{70}H_{57}N_3S.H_2O$: C 84.90, H 6,01, N 4.24; found: C 85.40, H 5.92, N 4.28.

15,20-Diphenyl-5,10-*p*-tolyl-2^1,2^4,7^1,7^4,12^1,12^4-hexahydro-2^1,2^4;7^1,7^4;12^1,12^4-triethano-22*H*,24-thiatetrabenzo[*b*,*g*,*l*]porphyrin (3BCODN): The reaction of **5b** with **2a** and *p*-tolualdehyde was performed according to the general procedure. The target porphyrin was isolated by chromatography with 70% CH_2Cl_2/hexane as eluent and recrystallization from $CHCl_3$/MeOH in 22% yield as dark purple crystals: m.p. >130°C (decomp); ^{1}H NMR ($CDCl_3$): δ=9.53 (s, 2H), 8.25–8.07 (m, 8H), 7.83–7.78 (m, 6H), 7.66–7.59 (m, 4H), 6.61–6.21 (m, 6H), 3.51 (m, 2H), 3.47 (m, 2H), 3.26 (m, 2H), 2.79 (s, 6H), 1.81–0.89 (m, 12H), −3.47 ppm (brs, 1H); MS (FAB): *m*/*z* (%): 894 (100) $[M+H]^+$, 866 (7), 838 (8), 810 (43); UV/Vis (CH_2Cl_2) λ_{max} (lgε)=426 (5.27), 518 (4.37), 616 (3.63), 674 nm (3.37); elemental analysis calcd (%) for $C_{64}H_{51}N_3S.H_2O$: C 84.27, H 5.86, N 4.61; found: C 84.07, H 5.80, N 4.57.

General procedure for preparative retro-Diels–Alder reaction: Expansion of the π system by thermal transformation of the fused BCOD groups into benzo moieties was carried out under the conditions reported previously (230–250°C, 30 min, ca. 0.2 mmHg).[11a] The products obtained are shown in Figure 1 with their carbon numbering schemes.[33] The precursor BCOD-fused porphyrin was placed in a sample tube in a 25 mL round-bottomed flask. The flask was then evacuated with a rotary vacuum pump and heated at 230°C for 30 min (*meso*-unsubstituted precursors) or for 1 h (*meso*-tetraaryl precursors) in a glass tube oven. After the mixture was cooled, the target core-modified benzoporphyrin was obtained in quantitative yield. The mechanism of the retro-Diels–Alder reaction was explored further for **TPS2N2**, **TPSN3**, **2BN**, and **2BS** by thermogravimetric analysis (see Figure S8 in the Supporting Information).

5,20-Diphenyl-10,15-*p*-tolyl-23*H*,21-thiatetrabenzo[*b*,*g*,*l*,*q*]porphyrin (TPSN3): green crystals; m.p. >300°C; ^{1}H NMR ($CDCl_3$): δ=8.27 (m, 4H, *o*-Ph), 8.19 (m, 4H; 2′,6′-positions of tolyl), 7.91 (m, 4H; *p*-Ph, H2^2, H2^3), 7.87 (m, 4H; *m*-Ph), 7.63 (m, 4H; 3′,5′-positions of tolyl), 7.42 (m, 2H; H2^1, H2^4), 7.34 (m, 2H; H12^1, H12^2), 7.26 (m, 2H; H12^2, H12^3), 7.15–7.11 (m, 4H; H7^2, H7^3, H17^2, H17^3), 6.91 (m, 2H; H7^4, H17^1), 6.86 (m, 2H; H7^1, H17^4), 2.77 (s, 6H), −0.38 ppm (brs, 1H); ^{13}C NMR ($CDCl_3$) δ 152.6, 147.7, 141.9, 140.4, 140.1, 139.3, 139.1, 138.9, 138.6, 134.2, 133.0, 132.9, 132.8, 129.5, 129.2, 128.8, 127.4, 125.9, 125.6, 125.5, 125.4, 125.3, 124.3, 123.9, 123.0, 120.8, 21.8 ppm; MS (FAB): *m*/*z*: 860 $[M+H]^+$; UV/Vis (CH_2Cl_2): λ_{max} (lgε)=477 (5.37), 607 (4.15), 652 (4.57), 669 (4.54), 720 nm (3.71); elemental analysis calcd (%) for $C_{62}H_{41}N_3S$: C 86.58, H 4.80, N 4.89; found: C 86.37, H 4.93, N 4.83.

5,10,15,20-Tetraphenyl-21,23-dithiatetrabenzo[*b*,*g*,*l*,*q*]porphyrin (TPS2N2): green crystals; m.p. >300°C; ^{1}H NMR ($CDCl_3$): δ=8.33 (m, 8H; *o*-Ph), 7.92 (m, 4H; *p*-Ph), 7.88 (m, 8H; *m*-Ph), 7.83 (m, 4H; H2^1, H2^4, H12^1, H12^4), 7.35 (m, 4H; H2^2, H2^3, H12^2, H12^3), 7.16 (m, 4H; H7^2, H7^3, H17^2, H17^3), 6.89 ppm (m, 4H; H7^1, H7^4, H17^1, H17^4); ^{13}C NMR ($CDCl_3$): δ=151.3, 142.3, 140.3, 140.1, 139.7, 133.1, 130.2, 129.3, 129.0, 126.1, 125.4, 123.5 ppm; MS (FAB): *m*/*z*: 849 $[M+H]^+$; UV/Vis (CH_2Cl_2): λ_{max} (lgε)=485 (5.28), 661 (4.57), 749 nm (3.49); elemental analysis calcd (%) for $C_{60}H_{36}N_2S_2$: C 84.87, H 4.27, N 3.30; found: C 84.70, H 4.55, N 3.25.

15,20-Diphenyl-5,10-*p*-tolyl-22H,24-thiatribenzo[*b*,*g*,*l*]porphyrin (3BN): purple crystals; m.p. >300°C; ^{1}H NMR: δ=9.33 (s, 2H; H17 and H18), 8.25 (m, 4H; *o*-Ph), 8.19 (m, 4H; 2′,6′-positions of tolyl), 7.86 (m, 6H; *m*-Ph, *p*-Ph), 7.66 (m, 4H; 3′,5′-positions of tolyl), 7.46–7.37 (m, 4H; H7^1, H7^2, H7^3, H7^4), 7.26 (m, 2H; H2^2, H12^2), 7.20 (m, 2H; H2^3, H12^3), 7.19 (m, 2H; H2^1, H12^4), 6.86 (m, 2H; H2^4, H12^1), 2.81 (s, 6H), −1.68 ppm (brs, 1H); ^{13}C NMR ($CDCl_3$): δ=152.2, 149.1, 145.9, 141.4, 140.8, 140.4, 140.1, 138.7, 135.1, 135.0, 134.2, 132.8, 131.8, 129.8, 129.6, 128.3, 128.2, 126.3 (2C), 125.7, 125.4, 124.6, 122.9, 116.8, 21.8 ppm; MS (FAB): *m*/*z*: 810 $[M+H]^+$; UV/Vis (CH_2Cl_2): λ_{max} (lgε)=454 (5.51), 550 (4.21), 584 (4.31), 644 (3.78), 705 nm (3.46); elemental analysis calcd (%) for $C_{58}H_{39}N_3S$: C 86.00, H 4.85, N 5.19; found: C 85.97, H 5.01, N 5.12.

5,10,15,20-Tetraphenyl-21,23-dithiadibenzo[*b*,*l*]porphyrin (2BS): green crystals; m.p. >300°C; ^{1}H NMR ($CDCl_3$): δ=8.34 (s, 4H; H7, H8, H17, H18), 8.18 (m, 8H; *o*-Ph), 8.05 (m, 4H; H2^1, H2^4, H12^1, H12^4), 7.87 (m, 4H; *p*-Ph), 7.83 (m 8H; *m*-Ph), 7.59 ppm (m, 4H; H2^2, H2^3, H12^2, H12^3); ^{13}C NMR ($CDCl_3$, typical signals): δ=150.6, 146.8, 142.2, 141.5, 134.1, 132.1, 131.7, 128.4, 128.0, 126.5, 124.1 ppm; MS (FAB): *m*/*z*: 749 $[M+H]^+$; UV/Vis (CH_2Cl_2): λ_{max} (lgε)=464 (5.28), 586 (3.95), 636 (4.46), 661 (4.13), 724 nm (3.46); elemental analysis calcd (%) for $C_{52}H_{32}N_2S_2$: C 83.39, H 4.31, N 3.74; found: C 83.23, H 4.42, N 3.69.

5,10,15,20-Tetraphenyl-22,24-dithiadibenzo[*b*,*l*]porphyrin (2BN): red crystals; m.p. >300°C; ^{1}H NMR ($CDCl_3$): δ=9.38 (s, 4H; H7, H8, H17, H18), 8.16 (m, 8H; *o*-Ph), 7.89 (m, 4H; *p*-Ph), 7.86 (m, 8H; *m*-Ph), 7.37 (m, 4H; H2^2, H2^3, H12^2, H12^3), 7.20 ppm (m, 4H; H2^1, H2^4, H12^1, H12^4); ^{13}C NMR ($CDCl_3$): δ=150.6, 146.8, 142.2, 141.5, 134.1, 132.1, 131.7, 128.4, 128.0, 126.5, 124.1 ppm; MS (FAB): *m*/*z*: 749 $[M+H]^+$; UV/Vis (CH_2Cl_2): λ_{max} (lgε)=439 (5.63), 516 (4.57), 544 (4.11), 641 (3.35), 703 nm (3.45); elemental analysis calcd (%) for $C_{52}H_{32}N_2S_2$: C 83.39, H 4.31, N 3.74; found: C 83.18, H 4.50, N 3.65.

5,20-Diphenyl-10,15-di-*p*-tolyl-23*H*,21-thiabenzo[*b*]porphyrin (1BS): purple crystals; m.p. >300°C; ^{1}H NMR ($CDCl_3$, assignments with asterisks are interchangeable): δ=8.57 (s, 2H; H12 and H13), 8.38 (m, 2H; H7, H18),* 8.16 (m, 2H; H8, H17)*, 8.05 (m, 4H; *o*-Ph), 7.99 (m, 4H; 2′, 6′-positions of tolyl), 7.97 (m, 2H; H2^1, H2^4), 7.82 (m, 2H; *p*-Ph), 7.79 (m, 4H; *m*-Ph), 7.60 (m, 2H; H2^2, H2^3), 7.50 (m, 4H; 3′,5′-positions of tolyl), 2.66 (s, 6H), −0.36 ppm (brs, 1H); ^{13}C NMR ($CDCl_3$): δ=160.7, 152.7, 142.5, 142.0, 140.6, 138.8, 138.3, 137.5, 135.1, 133.6, 131.8, 131.5,

128.1 (2C), 127.9, 127.8, 127.2, 127.0, 126.3, 125.5, 21.4 ppm; MS (FAB): m/z: 710 $[M+H]^+$; UV/Vis (CH_2Cl_2): λ_{max} ($\lg\varepsilon$) = 437 (5.45), 533 (4.13), 572 (4.17), 610 (3.70), 669 nm (3.43); elemental analysis calcd (%) for $C_{50}H_{35}N_3S$: C 84.59, H 4.97, N 5.92; found: C 84.58, H 5.14, N 5.84.

5,10,15,20-Tetraphenyltetrabenzo[*b*,*g*,*l*,*q*]porphyrin (TPTBP): Synthesis of TPTBP was based on the procedure reported previously by Luk'yanets and co-workers.[27] ^{1}H NMR ($CDCl_3$, −50 °C): δ = 8.41 (m, 8H; *o*-Ph), 7.97 (m, 4H; *p*-Ph), 7.89 (m, 8H; *m*-Ph), 7.43 (H2^1, H2^4, H12^1, H12^4), 7.35 (H2^2, H2^3, H12^2, H12^3), 7.18 (H7^2, H7^3, H17^2, H17^3), 6.99 (H7^1, H7^4, H17^1, H17^4), −1.34 ppm; ([D$_6$]DMSO, 100 °C): δ = 8.28 (m, 8H; *o*-Ph), 7.99 (m, 4H; *p*-Ph), 7.92 (m, 8H; *m*-Ph), 7.27 (m, 8H; δ protons), 7.17 (m, 8H; γ protons), −0.93 ppm (br, 2H); ^{13}C NMR ($CDCl_3$, −50 °C): δ = 148.6, 141.3, 139.6, 134.2, 133.2, 131.1, 129.0, 128.9, 126.2, 125.5, 124.4, 123.6, 115.4 ppm.

X-ray crystal structure analysis: X-ray structures were determined for **TPS2N2**, **TPSN3**, **1BS**, **2BS**, **2BN**, and **3BN**. Single crystals were prepared by slow evaporation of the solvent from saturated $CHCl_3$ solution or by diffusion of methanol into a solution of the compound in $CHCl_3$. With the exception of **3BN**, the crystals were collected by rapid filtration and mounted on top of glass fibers. A single crystal of **3BN** was placed in a Lindeman capillary tube with a very small amount of mother liquor and then the capillary was sealed by candle flame. Determination of the cell parameters and collection of the reflection intensities was performed on a Rigaku Mercury-7 (12 kW rotating anode generator) or a Mercury-8 (3 kW sealed tube) instrument equipped with graphite-monochromated $Mo_{K\alpha}$ radiation. The data were corrected for Lorentzian, polarization, and absorption effects. The structures were solved by direct methods (SIR-97[35] or SHELXS-97[36]) and expanded using the Fourier technique.[37] Hydrogen atoms were placed in calculated positions and refined by using riding models. All calculations were performed by using the CrystalStructure software package[38] or WinGX.[39] SHELXL-97[36] was used for structure refinement. In the case of **TPS2N2**, the reflection intensities were modified by the PLATON squeeze program[40] to remove the effect of poorly modeled solvent molecules.

TPS2N2: crystal formula: $C_{62}H_{40}N_2S{\cdot}1.5\,CHCl_3$, 0.12 × 0.06 × 0.03 mm, monoclinic, space group $P2_1/n$, a = 19.744(3), b = 10.2162(11), c = 24.538(3) Å, β = 101.260(3)°, V = 4854.2(11) Å^3, T = 83.1 K, Z = 4, ρ_{calcd} = 1.407 g cm^{-3}, μ = 0.402 mm^{-1}, F(000) = 2116, 49771 measured, 10858 unique, 7405 observed reflections [$I > 2\sigma(I)$]; R_1 = 0.0690 [$I > 2\sigma(I)$], wR_2 = 0.1890 (all data); GOF = 1.000.

TPSN3: crystal formula: $C_{62}H_{41}N_3S{\cdot}1.5\,CHCl_3$, 0.5 × 0.4 × 0.1 mm, monoclinic, space group $P2_1/n$, a = 19.4041(11), b = 10.8390(5), c = 24.7401(16) Å, β = 99.947(3)°, V = 5125.1(5) Å^3, T = 123.1 K, Z = 4, ρ_{calcd} = 1.347 g cm^{-3}, μ = 0.343 mm^{-1}, F(000) = 2148. The structure was refined without the solvent molecules by SHELXL-97 and Platon Squeeze. Refined formula $C_{62}H_{41}N_3S$, 40751 measured, 11650 unique, 8505 observed reflections [$I > 2\sigma(I)$]; R_1 = 0.0937 [$I > 2\sigma(I)$], wR_2 = 0.2425 (all data); GOF = 1.174.

1BS: crystal formula: $C_{50}H_{35}N_3S$, 0.60 × 0.25 × 0.10 mm, monoclinic, space group $P2_1/c$, a = 19.417(11), b = 9.398(5), c = 21.434(12) Å, β = 109.706(3)°, V = 3682(4) Å^3, T = 150 K, Z = 4, ρ_{calcd} = 1.28 g cm^{-3}, μ = 0.129 mm^{-1}, F(000) = 1488, 27338 measured, 8411 unique, 6162 observed reflections [$I > 2\sigma(I)$]; R_1 = 0.0895 [$I > 2\sigma(I)$], wR_2 = 0.2332 (all data); GOF = 1.130.

2BS: crystal formula: $C_{52}H_{32}N_2S_2$, 0.40 × 0.15 × 0.08 mm) Monoclinic, space group $P2_1/n$, a = 14.647(3), b = 6.1016(10), c = 20.221(3) Å, β = 94.260(4)°, V = 1802.2(5) Å^3, T = 103 K, Z = 2, ρ_{calcd} = 1.380 g cm^{-3}, μ = 0.191 mm^{-1}, F(000) = 780, 18282 measured, 4070 unique, 3123 observed reflections [$I > 2\sigma(I)$]; R_1 = 0.0420 [$I > 2\sigma(I)$], wR_2 = 0.1050 (all data); GOF = 1.016.

2BN: crystal formula: $C_{52}H_{32}N_2S_2$, 0.45 × 0.07 × 0.05 mm) Monoclinic, space group $P2_1/n$, a = 13.573(5), b = 9.204(3), c = 15.200(5) Å, β = 94.352(9)°, V = 1893.4(11) Å^3, T = 296 K, Z = 2, ρ_{calcd} = 1.314 g cm^{-3}, μ = 0.182 mm^{-1}, F(000) = 780, 18950 measured, 4292 unique, 2418 observed reflections [$I > 2\sigma(I)$]; R_1 = 0.0590 [$I > 2\sigma(I)$], wR_2 = 0.1410 (all data); GOF = 1.004.

3BN: crystal formula: $C_{58}H_{39}N_3S{\cdot}3\,CHCl_3$, 0.50 × 0.30 × 0.20 mm, triclinic, space group $P\bar{1}$, a = 12.524(4), b = 13.812(4), c = 16.809(6) Å, α = 77.831(11), β = 86.020(14), γ = 73.851(10)°, V = 2730.0(15) Å^3, T = 150 K, Z = 2, ρ_{calcd} = 1.421 g cm^{-3}, μ = 0.544 mm^{-1}, F(000) = 1196, 31980 measured, 12523 unique, 8936 observed reflections [$I > 2\sigma(I)$]; R_1 = 0.0669 [$I > 2\sigma(I)$], wR_2 = 0.1683 (all data); GOF = 1.049.

CCDC-637699 (**TPS2N2**), CCDC-637698 (**TPSN3**), CCDC-637703 (**1BS**), CCDC-637701 (**2BS**), CCDC-637702 (**2BN**) and CCDC-637700 (**3BN**) contain the supplementary crystallographic data for this paper. These data can be obtained free of charge from The Cambridge Crystallographic Data Centre via www.ccdc.cam.ac.uk/data_request/cif.

Calculations: Molecular structures were refined for **TPP**, **TBP**, **SN3**, **ON3**, **S2N2**, **OSN2**, **CN3**, **CSN2**, **TPS2N2**, **TPSN3**, **1BS**, **2BS**, **2BN**, and **3BN** with the Gaussian 03[41] and CAChe workstation (Fujitsu America Inc.) software packages.[42] **TPSN3**, **TPS2N2**, **1BS**, **3BN**, **2BN**, and **2BS** are predicted to be saddled into nonplanar geometries. Additional calculations were performed for the X-ray structures of **TPS2N2**, **TPSN3**, **1BS**, **3BN**, **2BN** and **2BS**.

Cyclic and differential pulse voltammetry: CV and DPV measurements were made on a Hokuto Denko HZ5000 potentiostat under purified nitrogen in *o*-dichlorobenzene (Nakalai Tesque) solutions with tetrabutylammonium perchlorate (TBAP, 0.1 M) as supporting electrolyte.

NMR spectroscopy: ^{1}H and ^{13}C NMR spectra were recorded on a JEOL JNM-AL 400 or -EX 400 spectrometer with tetramethylsilane as an internal standard.

Acknowledgement

This research was partially supported by the Ministry of Education, Science, Sports and Culture, Japan through a Grant-in-Aid for Exploratory Research (No. 19655045 to N.K.), a Grant-in-Aid for the COE project, Giant Molecules and Complex Systems, 2006 (to N.K.) and by Grant-in-Aids for the Scientific Research B and C (17350022 to H.U. and 18550036 to N.O., respectively), and for Young Scientists B (16750037 to T.O.). Partial financial support from the Mitsubishi Chemical Co. (to N.O.) is also acknowledged. We thank NSERC of Canada for Operating and Equipment grants (to M.J.S) and support from Fujitsu America Inc. in providing the CAChe Workstation software. We thank the Research Center for Molecular-Scale Nanoscience at the Institute for Molecular Science in Okazaki, Japan for permission (to N.O.) to carry out the X-ray measurements (Mercury-7). M.J.S. is a member of the Centre for Chemical Physics at UWO. Some of the computational results were obtained using the supercomputing resources at the Information Synergy Center at Tohoku University.

[1] S. Pervaiz, M. Olivio, *Clinic. Exper. Pharm. Physiol.* **2006**, *33*, 551–556.
[2] K. S. Suslick, C.-T. Chen, . G. R. Meredith, L.-T. Cheng, *J. Am. Chem. Soc.* **1992**, *114*, 6928–6930.
[3] J. Takeda, M. Sato, *Chem. Pharm. Bull.* **1994**, *42*, 1005–1007.
[4] E. D. Sternberg, D. Dolphin, C. Brückner, *Tetrahedron* **1998**, *54*, 4151–4202.
[5] T. D. Lash, *The Porphyrin Handbook, Vol. 2*, (Eds.: K. M. Kadish, K. M. Smith, R. Guilard) Academic Press, New York, **2000**, Chap. 10, pp. 125–199.
[6] L. Latos-Grażyński, *The Porphyrin Handbook, Vol. 2*, (Eds.: K. M. Kadish, K. M. Smith, R. Guilard) Academic Press, New York, **2000**, pp. 362–416.
[7] H. Uno, K. Nakamoto, K. Kuroki, A. Fujimoto, N. Ono, *Chem. Eur. J.* **2007**, *13*, 5773–5784.
[8] S. Ito, H. Uno, H. Watanabe, T. Murashima, N. Ono, Y. C. Tsai, R. G. Compton, *Tetrahedron Lett.* **2001**, *42*, 707–710.
[9] Y. Shimizu, Z. Shen, S. Ito, H. Uno, J. Daub, N. Ono, *Tetrahedron Lett.* **2002**, *43*, 8485–8488.
[10] a) S. Ito, T. Murashima, N. Ono, *J. Chem. Soc. Perkin Trans. 1* **1997**, 3161–3165; b) S. Ito, N. Ochi, T. Murashima, H. Uno, N. Ono, *Het-*

erocycles **2000**, *52*, 399–411; c) T. Okujima, N. Komobuchi, H. Uno, N. Ono, *Heterocycles* **2006**, *67*, 255–267.
[11] a) Y. Shimizu, Z. Shen, T. Okujima, H. Uno, N. Ono, *Chem. Commun.* **2004**, 374–375; b) T. Okujima, N. Komobuchi, Y. Shimizu, H. Uno, N. Ono, *Tetrahedron Lett.* **2004**, *45*, 5461–5464.
[12] A. Ulman, J. Manassen, *J. Am. Chem. Soc.* **1975**, *97*, 6540–6544.
[13] M. J. Broadhurst, R. Grigg, A. W. Johnson, *J. Chem. Soc. C*, **1971**, 3681–3690.
[14] a) R. E. Haddad, S. Gazeau, J. Pécaut, J.-C. Marchon, C. J. Medforth, J. A. Shelnutt, *J. Am. Chem. Soc.* **2003**, *125*, 1253–1268; b) C. J. Medforth, R. E. Haddad, C. M. Muzzi, N. R. Dooley, L. Jaquinod, D. C. Shyr, D. J. Nurco, M. M. Olmstead, K. M. Smith, J.-G. Ma, J. A. Shelnutt, *Inorg. Chem.* **2003**, *42*, 2227–2241; c) H. Ryeng, A. Ghosh, *J. Am. Chem. Soc.* **2002**, *124*, 8099–8103; d) A. K. Wertsching, A. S. Koch, S. G. DiMagno, *J. Am. Chem. Soc.* **2001**, *123*, 3932–3939.
[15] J. Mack, Y. Asano, N. Kobayashi, M. J. Stillman, *J. Am. Chem. Soc.* **2005**, *127*, 17697–17711.
[16] a) T. D. Lash, P. Chandrasekar, *J. Am. Chem. Soc.* **1996**, *118*, 8677–8678; b) J. D. Spence, T. D. Lash, *J. Org. Chem.* **2000**, *65*, 1530–1539; c) T. D. Lash, *J. Porphyrins Phthalocyanines* **2001**, *5*, 267–288; d) H. J. Xu, Z. Shen, T. Okujima, N. Ono, X. Z. Zhou, *Tetrahedron Lett.* **2006**, *47*, 931–934.
[17] J. Mack, M. J. Stillman, N. K. Kobayashi, *Coord. Chem. Rev.* **2007**, *251*, 429–453.
[18] M. Seth, T. Ziegler, A. Banerjee, J. Autschbach, S. J. A. van Gisbergen, E. J. Baerends, *J. Chem. Phys.* **2004**, *120*, 10942–10954.
[19] a) J. Michl, *J. Am. Chem. Soc.* **1978**, *100*, 6801–6811; b) J. Michl, *Pure Appl. Chem.* **1980**, *52*, 1549–1563.
[20] M. Gouterman, *The Porphyrins, Vol. III* (Ed.: D. Dolphin) Academic Press, New York, **1978**, pp.1-165.
[21] a) W. Moffitt, *J. Chem. Phys.* **1954**, *22*, 320–333; b) W. Moffitt, W. *J. Chem. Phys.* **1954**, *22*, 1820–1829.
[22] R.-J. Cheng, Y.-R. Chen, S. L. Wang, C. Y. Cheng, *Polyhedron* **1993**, *12*, 1353–1360.
[23] a) R. Bonnett, R. F. C. Brown, R. G. Smith, *J. Chem. Soc. Perkin Trans. 1* **1973**, 1432–1436; b) M. H. Palmer, S. M. F. Kennedy, *J. Chem. Soc. Perkin Trans. 2* **1976**, 81–89.
[24] T. Itoh, T. Murashima, H. Uno, N. Ono, *J. Chem. Soc. Chem. Commun.* **1998**, 1661–1662.
[25] R.-J. Cheng, Y.-R. Chen, C. C. Chen, *Heterocycles* **1994**, *38*, 1465–1469.
[26] P. S. Clezy, A. H. Mirza, *Aust. J. Chem.* **1982**, *35*, 197–209.
[27] E. A. Luk'yanets, S. N. Dashkevich, N. Kobayashi, *Russ. J. Gen. Chem.* **1993**, *63*, 985–988.
[28] a) J. D. Keegan, A. M. Stolzenberg, Y. C. Lu, R. E. Linder, G. Barth, A. Moscowitz, E. Bunnenberg, C. Djerassi, *J. Am. Chem. Soc.* **1982**, *104*, 4305–4317; b) J. D. Keegan, A. M. Stolzenberg, Y. C. Lu, R. E. Linder, G. Barth, A. Moscowitz, E. Bunnenberg, C. Djerassi, *J. Am. Chem. Soc.* **1982**, *104*, 4317–4329; c) C. Djerassi, Y. Lu, A. Waleh, A. Y. L. Shu, R. A. Goldbeck, L. A. Kehres, C. W. Crandell, A. G. H. Wee, A. Kniezinger, R. Gaete-Holmes, G. H. Loew, P. S. Clezy, E. Bunnenberg, *J. Am. Chem. Soc.* **1984**, *106*, 4241–4258.
[29] G. C. Chen, J. T. Yang, *Anal. Lett.* **1977**, *10*, 1195–1207.
[30] a) K. Smith, *The Porphyrin Handbook, Vol. 1*, (Eds.: K. M. Kadish, K. M. Smith, R. Guilard) Academic Press **2000**, pp. 1–43; b) J. S. Lindsey, *The Porphyrin Handbook, Vol. 1*, (Eds.: K. M. Kadish, K. M. Smith, R. Guilard) Academic Press **2000**, pp. 45–118.
[31] Z. Arnold, *Collect. Czech. Chem. Commun.* **1965**, *30*, 2783–2791.
[32] D. Stephan, A. Gorgues, A. Le Coq, *Tetrahedron Lett.* **1986**, *27*, 4295–4298.
[33] G. P. Moss, *Eur. J. Biochem.* **1988**, *178*, 277–328.
[34] E. S. Corey, I. N. Marina, G. H. David, R. D. Sherry, O. G. Sandra, R. O. Allan, L. G. Scott, H. Russell, R. D. Michael, *J. Med. Chem.* **2000**, *43*, 2403–2410.
[35] A. Altomare, M. C. Burla, M. Camalli, G. Cascarano, C. Giacovazzo, A. Guagliardi, A. G. G. Moliterni, G. Polidori, R. Spagna, *J. Appl. Crystallogr.* **1999**, *32*, 115–119.
[36] G. Sheldrick, T. Schneider, *Methods Enzymol.* **1997**, *277*, 319–343.
[37] P. T. Beurskens, G. Admiraal, G. Beurskens, W. P. Bosman, R. de Gelder, R. Israel, J. M. M. Smits, *Technical Report of the Crystallography Laboratory* **1999**, University of Nijmegen, The Netherlands.
[38] CrystalStructure Ver. 3.7.0, Crystal Structure Analysis Package, Rigaku (3-9-12 Akishima, Tokyo, Japan) and Rigaku/MSC (9009 New Trails Dr., The Woodlands, TX 77381 USA), (2000–2004).
[39] L. J. Farrugia, *J. Appl. Crystallogr.* **1999**, *32*, 837–838.
[40] A. L. Spek, *J. Appl. Crystallogr.* **2003**, *36*, 7–13.
[41] Gaussian 03 (Revision C.02), M. J. Frisch, G. W. Trucks, H. B. Schlegel, G. E. Scuseria, M. A. Robb, J. R. Cheeseman, J. A. Montgomery, Jr., T. Vreven, K. N. Kudin, J. C. Burant, J. M. Millam, S. S. Iyengar, J. Tomasi, V. Barone, B. Mennucci, M. Cossi, G. Scalmani, N. Rega, G. A. Petersson, H. Nakatsuji, M. Hada, M. Ehara, K. Toyota, R. Fukuda, J. Hasegawa, M. Ishida, T. Nakajima, Y. Honda, O. Kitao, H. Nakai, M. Klene, X. Li, J. E. Knox, H. P. Hratchian, J. B. Cross, V. Bakken, C. Adamo, J. Jaramillo, R. Gomperts, R. E. Stratmann, O. Yazyev, A. J. Austin, R. Cammi, C. Pomelli, J. W. Ochterski, P. Y. Ayala, K. Morokuma, G. A. Voth, P. Salvador, J. J. Dannenberg, V. G. Zakrzewski, S. Dapprich, A. D. Daniels, M. C. Strain, O. Farkas, D. K. Malick, A. D. Rabuck, K. Raghavachari, J. B. Foresman, J. V. Ortiz, Q. Cui, A. G. Baboul, S. Clifford, J. Cioslowski, B. B. Stefanov, G. Liu, A. Liashenko, P. Piskorz, I. Komaromi, R. L. Martin, D. J. Fox, T. Keith, M. A. Al-Laham, C. Y. Peng, A. Nanayakkara, M. Challacombe, P. M. W. Gill, B. Johnson, W. Chen, M. W. Wong, C. Gonzalez, J. A. Pople, Gaussian, Inc., Wallingford, CT, **2004**.
[42] CAChe Scientific, P.O. Box 500, Mail Station 13-400, Beaverton, Oregon 97077.

Received: October 12, 2007
Revised: January 19, 2008
Published online: April 16, 2008

